



**STRUCTURAL SYSTEMS
RESEARCH PROJECT**

Report No.
SSRP-16/07
CFS Test Program
Report #1

**Earthquake and fire performance of
a mid-rise cold-formed steel framed
building – test program and test
results: *Rapid Release Report***

by

**Xiang Wang, Tara Hutchinson, Gilbert Hegemier,
Srikar Gunisetty
(UCSD)**

**Praveen Kamath, Brian Meacham
(WPI)**

December 2016

Department of Structural Engineering
University of California, San Diego
La Jolla, California 92093-0085

University of California, San Diego
Department of Structural Engineering
Structural Systems Research Project
Report No. SSRP-16/07

**Earthquake and fire performance of a mid-rise cold-formed steel framed
building – test program and test results: *Rapid Release Report***
by

Xiang Wang, Tara Hutchinson, Gilbert Hegemier, Srikar Gunisetty
(University of California, San Diego)

Praveen Kamath, Brian Meacham
(Worcester Polytechnic Institute)

Department of Structural Engineering
University of California, San Diego
La Jolla, California 92093-0085
December 2016

DISCLAIMER

The work that provided the basis for this publication was supported by funding under a Grant with the U.S. Department of Housing and Urban Development, Office of Policy Development and Research. The substance and findings of the work are dedicated to the public. The author and publisher are solely responsible for the accuracy of the statements and interpretations contained in this publication. Such interpretations do not necessarily reflect the views of the Government.

ACKNOWLEDGEMENTS

This project is a collaboration between two academic institutions (University of California, San Diego and Worcester Polytechnic Institute), two government or institutional granting agencies (Department of Housing and Urban Development and the California Seismic Safety Commission) and more than fifteen industry partners (a complete list of industry sponsors may be found in Appendix A). It is noted that although UCSD led the overall test program, this team's primary focus was on the earthquake testing phases, while WPI's primary focus was on the fire testing phases. For sake of harmony and flow in the present report, herein both testing phases are presented. We also thank the Jacobs School of Engineering and Department of Structural Engineering at UCSD for matching support of this effort. Industry sponsors include the California Expanded Metal Products Co. (CEMCO) and Sure-Board, who each provided financial, construction, and materials support. Specific individuals that dedicated significant time on behalf of this effort included Fernando Sesma (CEMCO), Kelly Holcomb, Carleton Elliot and Tyler Elliot (Sure-Board), Harry Jones (DCI Engineers), Diego Rivera (SWS Panels), Doug Antuma (Rivante), Larry Stevig (State Farm Insurance), Tim Reinhold and Warner Chang (Insurance Institute for Business and Home Safety), Steve Helland (DPR Construction), Rick Calhoun (Walters & Wolf), and Jesse Karnes (MiTek). We appreciate the efforts of these individuals and their colleagues at their respective firms.

Regarding the test program, the technical support of NHERI@UCSD staff, namely, Robert Beckley, Jeremy Fitcher, Dan Radulescu, and Alex Sherman, are greatly appreciated. The authors are also grateful to Professor Yehuda Bock and graduate student Dara Goldberg from the Scripps Institute of Oceanography at UCSD for providing the Global Positioning System and related technical support, and Professor Falko Kuester and his students from the Department of Structural Engineering at UCSD for collecting aerial video footage and LiDAR image data of the test specimen. Experiments performed at the National Institute of Standards and Technology (NIST), led by Dr. Matthew Hoehler, supported the planning of this test program, and are greatly appreciated. Technical input to this report regarding the physical observations to appliances and other installed equipment were provided by Pat Boyer, Jack Jordan, and Larry Stevig of State Farm Insurance and Warner Chang of IBHS. These entities also kindly supplied appliances and provided support during the test program. In addition, the authors also greatly appreciate UCSD

Department of Environment, Health & Safety, and the San Diego Fire Department for providing the necessary approvals and fire department participation during the fire-testing phase of this effort. The above continuous support is gratefully acknowledged. Findings, opinions, and conclusions are those of the authors and do not necessarily reflect those of the sponsoring organizations.

EXECUTIVE SUMMARY

A substantial growth in the use of cold-formed steel (CFS) framed construction has recently been observed, notably in high seismic regions in the western United States. Structural systems of this kind consist of light-gauge framing members (e.g., studs, tracks, joists) attached with sheathing materials (e.g., wood, sheet steel). CFS-framed structures can offer lower installation and maintenance costs than other structural types, particularly when erected with prefabricated assemblies. They are also durable, formed of an inherently ductile material of consistent behavior, lightweight, and manufactured from recycled materials. Compared to other lightweight framing solutions, CFS is non-combustible, an important basic characteristic to minimize fire spread. While these lightweight systems provide the potential to support the need for resilient and sustainable housing, the state of understanding regarding their structural behavior in response to extreme events, in particular earthquakes and ensuing hazards, remains relatively limited.

To this end, a unique research collaboration between academia, government, and industry was formed to contribute to understanding the earthquake and post-earthquake fire behavior of mid-rise CFS-framed buildings. Led by the University of California, San Diego (UCSD), with partnerships from Worcester Polytechnic Institute, government and state agencies, and more than 15 industry sponsors, the centerpiece of this project involved full-scale earthquake and fire testing of a full-scale six-story CFS wall braced building. The test building was constructed on the world's largest outdoor shake table – the Large High Performance Outdoor Shake Table (LHPOST) at UCSD. Within a three-week test program, the building was subjected to seven earthquake tests of increasing motion intensity. Earthquake motions were scaled to impose service, design, and maximum credible earthquake (MCE) demands onto the test building. Subsequently, live fire tests were conducted on the earthquake-damaged building at two select floors. Finally, for the first time, the test building was subjected two post-fire earthquake tests, including a low-amplitude ‘aftershock’ and an extreme near-fault target MCE-scaled motion. In addition, low-amplitude white noise and ambient vibration data were collected during construction and seismic testing phases to support identification of the dynamic state of the building-NCS system.

During the earthquake test phases, the building was outfitted with more than 250 analog sensors, a Global Positioning System (GPS) system, and an array of more than 40 digital video cameras to record the behavior of the structural components and building. Between the two seismic test phases, thermocouples were installed in various locations of the fire test compartments. Sacrificial video cameras were also installed to collect visual data regarding smoke or fire spread. In addition, unmanned aerial vehicles (UAVs) were flown surrounding the test building at all phases (earthquake and fire) to capture its global response.

The present *rapid release* report is the first in a series devoted to this project. The intent of this report (released quickly following test completion) is to synthesize immediate understanding from the program and stimulate discussions for future data analysis/reporting that can support design efforts. Within this report, several initial findings relative to the system identification results, the seismic response of the building, the live fire tests, and the observed physical damage of the test building during this unique test program are presented. Systematic study of the experimental results is an ongoing effort. These results will be presented in the remaining reports in this series. The second report will present expanded analysis of the test results of the system-level structural behavior of the test building in earthquake and fire as well as the response of individual structural nonstructural components during the seismic tests, and a third report will provide supplemental materials regarding the test building design and construction as well as the test program.

TABLE OF CONTENTS

DISCLAIMER	i
ACKNOWLEDGEMENTS	ii
EXECUTIVE SUMMARY	iv
TABLE OF CONTENTS.....	vi
LIST OF FIGURES	viii
LIST OF TABLES	xi
1 INTRODUCTION	1
1.1 Overview of the Project	1
1.2 Scope of Present Rapid Release Report.....	1
1.3 Project Team	2
2 BUILDING DESIGN AND CONSTRUCTION	3
2.1 Building Design and Specimen Description	3
2.2 Structural Components.....	5
2.2.1 Shear Walls	6
2.2.2 Gravity Walls	7
2.2.3 Floor Diaphragm.....	8
2.3 Nonstructural Systems	9
2.3.1 Partition Walls	9
2.3.2 Doors.....	10
2.3.3 Appliances.....	13
2.4 Building Construction.....	16
3 TEST PROTOCOL	21
3.1 Pre-test Vibration Test Protocol.....	21
3.2 Earthquake Test Protocol.....	23
3.3 Fire Test Protocol.....	27
4 MONITORING SYSTEM.....	30

4.1	Earthquake Phase	30
4.2	Fire Test Phase	33
5	TEST RESULTS	39
5.1	System Identification Results	39
5.2	Earthquake Test Results	41
5.2.1	Peak Building Response	42
5.2.2	Residual Displacements	44
5.2.3	Acceleration Amplification	45
5.3	Fire Test Results	46
5.4	Physical Observation	53
5.4.1	Structural System	53
5.4.2	Nonstructural Systems	57
6	CONCLUSIONS	64
	REFERENCES	67
	APPENDIX A – PROJECT PARTICIPANTS	68
	APPENDIX B – SHAKE TABLE SPECIFICATIONS	70
	APPENDIX C – TEST DAY PROTOCOL	72

LIST OF FIGURES

Figure 2.1. Site-specific mapped spectral accelerations.	3
Figure 2.2. Test building: (a) isometric view, and (b) building plan layout (typical of floor 2 to 6, note that floor 1 is identical sans the transverse partition walls).	4
Figure 2.3. Corridor shear wall: (a) CFS framing (viewing from room side), and (b) tie-down assembly.....	7
Figure 2.4. Exterior non-shear gravity wall CFS framing (view from building interior).	8
Figure 2.5. Interior partition wall: (a) CFS framing, and (b) finished wall.	10
Figure 2.6. Plan layout of the doors (level 2, typical of levels 3-6).....	11
Figure 2.7. Photographs of the typical door types: (a) single-swing wood door (1.0 m \times 2.2 m), (b) single-swing metal door with a 20-minute fire rating (1.0 m \times 2.5 m), (c) double-swing wood door (2.0 m \times 2.5 m) (d) single-swing wood door with a side lite frame (1.6 m \times 2.5 m) (e) sliding door with a side lite frame (2.0 m \times 2.7 m).	11
Figure 2.8. Appliance plan layout: (a) level 1, and (b) level 6 (note the hatched pattern on level 6 delineates the outline of the mass plates, and elevated wood-framed platform was placed over the mass plates).	14
Figure 2.9. Photographs of appliances at level 1: (a) electric range units, (b) water heaters, and (c) gas piping assembly with seismic gas shutoff valves.....	15
Figure 2.10. Diaphragm panel pattern (top) and photographs of the prefabricated diaphragm segments prior to installation (bottom) (room segments #1 – #4 and corridor segments #5 and #6).	17
Figure 2.11. Prefabricated wall panel pattern (top) and sample photographs of prefabricated wall segments (bottom).....	18
Figure 2.12. Construction of the test building: (a) building tie-down system (photo taken on April 16, 2016), (b) in-situ installation of first-story wall system (photo taken on April 19, 2016), (c) installation of a prefabricated wall panel at the third story (photo taken on April 23, 2016), (d) completion of building skeleton erection (hoisting the last piece of roof panel) (photo taken on April 27, 2016), and (e) roof mass plate layout prior to the earthquake tests (photo taken on June 10, 2016).	20
Figure 3.1. Acceleration time histories of achieved input motions.	25
Figure 3.2. Displacement time histories of achieved input motions.....	26
Figure 3.3. Elastic response spectra of achieved motions ($\xi = 5\%$): (a) pseudo-acceleration spectra, and (b) displacement spectra.	26

Figure 3.4. Fire test sequence specified on the building plan layout (level 2 and level 6).....	28
Figure 3.5. Three-dimensional view of the fire compartments: (a) southwest compartment, (b) southeast compartment, (c) northwest compartment, and (d) corridor.....	29
Figure 4.1. Plan layout of accelerometers on the second floor.....	31
Figure 4.2. Plan layout of video cameras: (a) level 1, and (b) level 2.....	32
Figure 4.3. Thermocouple layout in the southwest compartment at level 2 and adjacent space associated with Fire Test 1.....	36
Figure 4.4. Thermocouple layout of the corridor at level 2 and adjacent space associated with Fire Test 4.....	37
Figure 5.1. Identified modal periods and damping ratios of the first longitudinal and torsional vibration modes of the test building during 3% g RMS WN tests.....	40
Figure 5.2. Identified mode shapes associated with the initial state (S0): (a) mode 1-L, and (b) mode 1-To.....	41
Figure 5.3. Building peak responses during <u>the service level tests</u> : (a) peak floor accelerations, and (b) peak interstory drift ratios.....	43
Figure 5.4. Building peak responses during <u>above-the-service-level</u> tests: (a) peak floor accelerations, and (b) peak interstory drift ratios.....	44
Figure 5.5. Time histories of the absolute displacement of the lower four floors and interstory drift ratio of the lower three levels during test EQ9.....	45
Figure 5.6. Acceleration amplification factor of the test building under: (a) <u>service level</u> tests, and (b) <u>above-the-service level</u> tests.....	46
Figure 5.7. Temperature response of the southwest compartment at level 2 (burn room) – Fire Test 1.....	49
Figure 5.8. Temperature response of the stud cavities in the southwest compartment at level 2 – Fire Test 1.....	49
Figure 5.9. Temperature response of the ceiling joist cavities above the southwest compartment at level 2 – Fire Test 1.....	50
Figure 5.10. Temperature response of the east end of the corridor at level 2 – Fire Test 4.....	51
Figure 5.11. Temperature response of the west end of the corridor at level 2 – Fire Test 4.....	51
Figure 5.12. Flame and smoke extension from the compartment openings: (a) Fire Test 1, and (b) Fire Test 4.....	52

Figure 5.13. Damage to the test building during the pre-fire earthquake test sequence: (a) gypsum bulging on the bottom edge (EQ2), (b) gypsum screw popping (EQ3), (c) buckled sheet steel of corridor shear wall at level 1 (EQ6), (d) sheathing panel crushing between the shear wall and gravity wall at level 4 corridor (EQ7), (e) buckled composite panel sheet steel of corridor shear wall at level 4(EQ7), and (f) buckled rim track flange above gravity wall at level 4 (EQ7).....	54
Figure 5.14. Damage to the test building following the fire tests: (a) level 2 corridor, (b) partially detached door, (c) partially detached gypsum ceiling, and (d) sagging floor system at the second floor.....	55
Figure 5.15. Damage of the test building at the completion of the test program: (a) severely damaged corridor shear wall at level 2, (b) dislodged tension rods at the corner shear wall at level 2 (southeast room), and (c) north façade of the building at the lower three levels with apparently residual drifts at level 2.	56
Figure 5.16. North elevation of the test building: (a) pre-EQ9 condition, and (b) pre-EQ9 condition.	57
Figure 5.17. Examples of door damage: (a) door frame screw popping (DS-1), (b) door frame gapping (DS-2), (c) buckled door latch (DS-2), and (d) detached door frame (DS-3).....	58
Figure B.1. UCSD Large High Performance Outdoor Shake Table (LHPOST).	70
Figure B.2. Schematic view of the LHPOST test facility (nheri.ucsd.edu).....	71

LIST OF TABLES

Table 2.1. Detailed descriptions of the doors.	12
Table 2.2. Appliances and their associated specifications.	13
Table 3.1. Low-amplitude vibration test sequence during construction phase.....	22
Table 3.2. White noise test sequence and the building configuration	22
Table 3.3. Seismic test protocol.....	23
Table 3.4. White noise test sequence and the associated building states.....	24
Table 3.5. Summary of select characteristics of achieved earthquake input motions	27
Table 3.6. Fire test protocol	28
Table 4.1. Analog sensor instrumentation plan during the earthquake tests	30
Table 4.2. Video camera system during the earthquake tests	31
Table 4.3. Summary of thermocouple instrumentation plan.....	35
Table 4.4. Video camera locations and their post-test conditions.	38
Table 5.1. Peak building responses during the earthquake tests	42
Table 5.2. Burn duration and achieved maximum temperature.....	47
Table 5.3. Door damage states and the associated damage modes.....	58
Table 5.4. Physical observations of door damage.....	59
Table 5.5. Physical observations of the range units during the pre-fire earthquake tests.....	61
Table 5.6. Physical observations of the water heaters during the pre-fire earthquake tests.	62
Table 5.7. Performance of the seismic gas shutoff valves during the pre-fire earthquake tests....	63
Table A.1. Project academic team	68
Table A.2. Government and institutional sponsors.....	68
Table A.3. Industrial sponsors	69
Table B.1. Shake table performance specifications	71

1 INTRODUCTION

1.1 Overview of the Project

To address the need for understanding the earthquake and post-earthquake fire behavior of mid-rise cold-formed steel (CFS) framed buildings, a unique multidisciplinary test project was conducted on the Large High Performance Outdoor Shake Table (LHPOST) at University of California, San Diego (UCSD) between April and July 2016. Central to this research was the system-level earthquake and live fire testing of a full-scale six-story CFS wall braced building. In a three-week test program, the building was subjected to seven earthquake tests of increasing motion intensity. Earthquake motions were scaled to impose service, design, and maximum credible earthquake (MCE) demands onto the test building. Subsequently, live fire tests were conducted on the earthquake-damaged building at two select floors. Finally, the test building was subjected two post-fire earthquake tests, including a low-amplitude ‘aftershock’ and an extreme near-fault target MCE intensity motion.

In parallel with the system-level building experiments, an experimental study was undertaken on six CFS framed shear wall specimens at the National Institute of Standards and Technology (NIST) in June 2016. The wall specimens in this study were constructed to replicate those of the test building. Specimens were subjected to a combination of reversed cyclic quasi-static loading and live thermal loads in an effort to understand the potential for degradation in wall capacity under earthquake-fire scenarios. Test results from this program are not presented herein, however, interested readers may refer to the report of Hoehler and Smith (2016).

1.2 Scope of Present Rapid Release Report

A rich set of data has emerged from these tests and within this rapid release report several initial impressions from the analysis of this data with regard specifically to system identification, the global seismic response of the building, the live fire tests, and the observed physical damage of the test building during this test program are presented. Systematic study of the experimental results is an ongoing effort, and thus these results will be expanded upon in a final report. However, the intent of the present, *rapid release* report, which is being released quickly following test completion, is to synthesize immediate impressions from the program and

stimulate discussions for future data analysis/reporting^[1,2] that can support design efforts. With an ultimate goal of achieving sustainable and resilient housing communities via the use of CFS-framed buildings, findings from this project will be important to the practitioners in several aspects: (i) evaluating the seismic and post-earthquake fire performance, (ii) supporting advancement of engineering models for use in current design practice, (iii) contributing to next-generation design codes, and (iv) improving construction and design practices.

1.3 Project Team

To realize this multidisciplinary experimental research project, two universities, two (one each federal and state) government agencies, non-profit granting agencies, and more than 15 industry partners participated. The academic team was comprised of faculty, postdoctoral and graduate researchers from the University of California, San Diego (lead academic institution) and Worcester Polytechnic Institute (Table A.1 in Appendix A). The Department of Housing and Urban Development and California Seismic Safety Commission, alongside numerous leading industry partners, provided the financial and material resources needed to support the testing program. The unique support and leadership of industry sponsors in this effort were essential to advancing the test program (Tables A.2 and A.3 in Appendix A).

¹Wang, X., Hutchinson, T.C., Hegemier, G., Gunisetty, S., Kamath, P., and Meacham, B. (2016). “Earthquake and fire performance of a mid-rise cold-formed steel framed building – test program and test results: *Final Report*.” *SSRP-2016/08*, Dept. of Structural Engineering, Univ. of California, San Diego.

² Wang, X., Hutchinson, T.C., Hegemier, G., and Gunisetty, S. (2016). “Earthquake and fire performance of a mid-rise cold-formed steel framed building – supplemental materials: *Final Report*.” *SSRP-2016/09*, Dept. of Structural Engineering, Univ. of California, San Diego.

2 BUILDING DESIGN AND CONSTRUCTION

2.1 Building Design and Specimen Description

The test building was designed as a CFS framed building in the high seismic region near downtown Los Angeles (coordinates: 34.0423N and 118.2641W). The hypothetical site corresponds to a NEHRP Site Class D (stiff soil) condition, with the mapped spectral accelerations of $S_{DS} = 1.53$ g and $S_{D1} = 0.81$ g (Figure 2.1). The overall building design complied with current code provisions within ASCE 7-10 *Minimum Design Loads for Buildings and Other Structures* (ASCE, 2010), AISI S100 *North American Specification for the Design of Cold-formed Steel Structural Members* (AISI, 2012), and AISI S213 *North American standard for cold-formed steel farming—Lateral design* (AISI, 2007).



Figure 2.1. Site-specific mapped spectral accelerations.

As shown in Figure 2.2, the six-story test building had a uniform plan dimension of 10.4 m \times 7.3 m (34 ft \times 24 ft) at each floor, occupying almost the entire 12.2 m \times 7.6 m (40 ft \times 25 ft) shake table footprint. The total height of the building was 19.2 m above the shake table platen (a floor-to-floor height of 3.1 m (10 ft) for all stories and a 1.2 m-tall (4 ft tall) parapet on the roof perimeter). The seismic design considered uniformly distributed dead and live loads of 1.5

kN/m^2 (32 psf) and 1.9 kN/m^2 (40 psf) at each floor (the live load on the roof was taken as 1.0 kN/m^2 (20 psf)). Consequently, the effective seismic design weight of the test building was assumed as 1420 kN (320 kips). According to ASCE 7-10 (ASCE, 2010), the CFS wall braced building was designed with a response modification factor R of 6.5, an overstrength factor Ω of 3.0, and a deflection amplification factor C_d of 4.0. The code-based fundamental period of the test building T was determined as 0.43 sec (considering a building height of 18.3 m (60 ft) excluding the height of the parapets). Consequently, the base shear coefficient C_s of the test building was determined as 0.236. This resulted in an effective seismic design base shear V_b of 334 kN (75 kips).

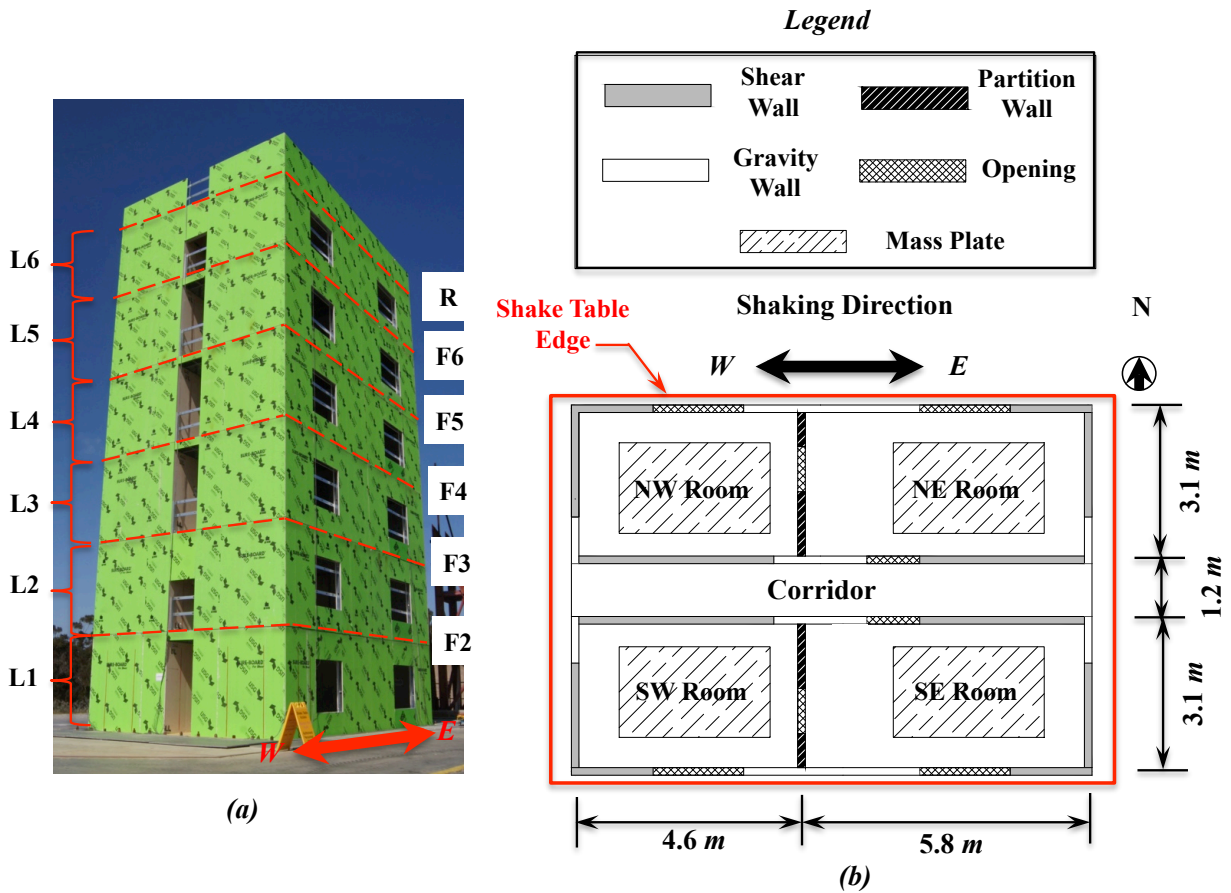


Figure 2.2. Test building: (a) isometric view, and (b) building plan layout (typical of floor 2 to 6, note that floor 1 is identical sans the transverse partition walls).

As shown in Figure 2.2b, the building had a symmetric floor plan with a 1.2 m (4 ft) wide corridor oriented along the longitudinal centerline and a room at each quadrant of the building. Two transverse partition walls were located 0.6 m (2 ft) west of the transverse centerline (level 2

through level 6), each separating the two rooms on the same side of the corridor. However, no partition walls were installed at the first level due to insufficient attachment condition to the shake table platen. The exterior façade of the building provided four partial-height window openings (one at each room) and two full-height corridor openings (at each end of the corridor) at each level (Figure 2.2a). Dropped (partial-height) soffits were constructed on the corridor openings at the level 2 and level 6 to attain the anticipated ventilation condition in the compartment fire tests. To account for the live loads and the weight of certain architectural features excluded from the construction (e.g., flooring, exterior façade finishing), four mass plates were installed on the floor diaphragm at each floor from the second floor through the roof (Figure 2.2b). Each of the mass plate had a dimension of 3.0 m \times 1.8 m (10 ft \times 6 ft) and an estimated weight of \sim 16.5 kN (3.7 kips).

The building was equipped with four doors at each level (one each on the two corridor walls and the two transverse partition walls) at level 2 through level 6 (Figure 2.2b). However, level 1 consisted of only two corridor doors due to the absence of partition walls. In addition, the building was outfitted with a variety of household appliances (e.g., gas and electric range units, water heaters, wall-mounted television sets, and etc.) at level 1 and level 6. The actual weight of the test building including its nonstructural components was \sim 1120 kN (250 kips) at the completion of building construction. It is noted that the actual test weight of the building was \sim 300 kN (70 kips) lower than its design weight, which was intended to account for the reduction of live loads (with a reduction factor of \sim 0.6) in the event of an earthquake.

2.2 Structural Components

The vertical structural system of the building consisted of steel sheathed, steel stud shear walls that were designed to resist both vertical and lateral loads as well as gravity walls, which formed the vertical load bearing system. The horizontal structural system solely consisted of (floor and roof) diaphragms that were designed to transfer the lateral and vertical loads to the vertical structural walls. In addition, a continuous rod tie-down system was integrated at the ends of shear walls to resist uplifting of the shear walls. The rod tie-down system was sandwiched between compression studs (welded CFS stud packs) to carry the alternative compression load during seismic events. Each major structural component is briefly described in the following subsections.

2.2.1 Shear Walls

As illustrated in Figure 2.2b, two longitudinal shear walls were placed along each (east and west) end of the corridor, with an associated wall length of 4.0 m (13 ft) for the walls at the west end and 3.3 m (11 ft) for those at the east end. In addition, L-shaped shear walls with a length of 1.6 m (5'-4") in the longitudinal direction and 2.1 m (7 ft) in the transverse direction were placed at each of the four corners of the building. The total shear wall length was 21.3 m (70 ft) in the longitudinal (shaking) direction and 8.6 m (28 ft) in the transverse direction. It is noted that the corridor shear walls were designed as the primary lateral load resisting elements for the building, while the corner shear walls were assumed to provide lateral resistance to transverse and torsion loads.

The shear wall framing was fabricated using standard CFS members (e.g., studs, tracks) (Figure 2.3a). Sheathing material consisted of composite structural panels sheathed on the exterior or corridor side and 16 mm (5/8") thick standard gypsum panels on the interior room side. The composite panels were fabricated using 16 mm (5/8") thick gypsum boards bonded with a layer of 0.686 mm (0.027") thick (22 ga.) sheet steel for improving the shear capacity of the panels. Vertical studs used 600S200-68 at 610 mm (24") o.c for the first level corridor walls and 600S200-54 at 610 mm (24") o.c for the corridor walls at all the remaining levels as well as the corner walls at all levels. With the exception of the first-story bottom tracks that used 600T200-97, all shear wall top and bottom tracks were made of 600T200-54. The composite structural panels of the corridor walls were attached to framing using #8 self-tapping metal screws at different spacing at different levels (76 mm (3") o.c. for the lower three levels, 102 mm (4") for level 4, and 152 mm (6") o.c for the upper two levels), while the screw spacing of 152 mm (6") o.c was consistently used for corner walls at all levels. Gypsum panels were attached to the studs and tracks by #8 drywall screws at a spacing of 152 mm (6") o.c. on boundary and 406 mm (16") o.c in field.

The building tie-down system was embedded within the shear wall framing and spanned continuously over all levels of the building to provide resistance to shear wall uplift. As shown in Figure 2.3a, a pair of tie-down subassemblies was placed at the wall ends, each consisting of continuous tension rods connected by couplers and a compression post made of built-up stud packs (Figure 2.3b). As the design uplift force reduces at a higher building level, the detailing of

the tie-down system varied considerably over the building height. The tension rods had a diameter of 45 mm (1-3/4") at the first level and progressively reduced to 16 mm (5/8") at the sixth level. In addition, the compression post built-up sections of the corridor walls composed of (10) 600S200-97 at the first level but only (4) 600S200-54 at the sixth level.

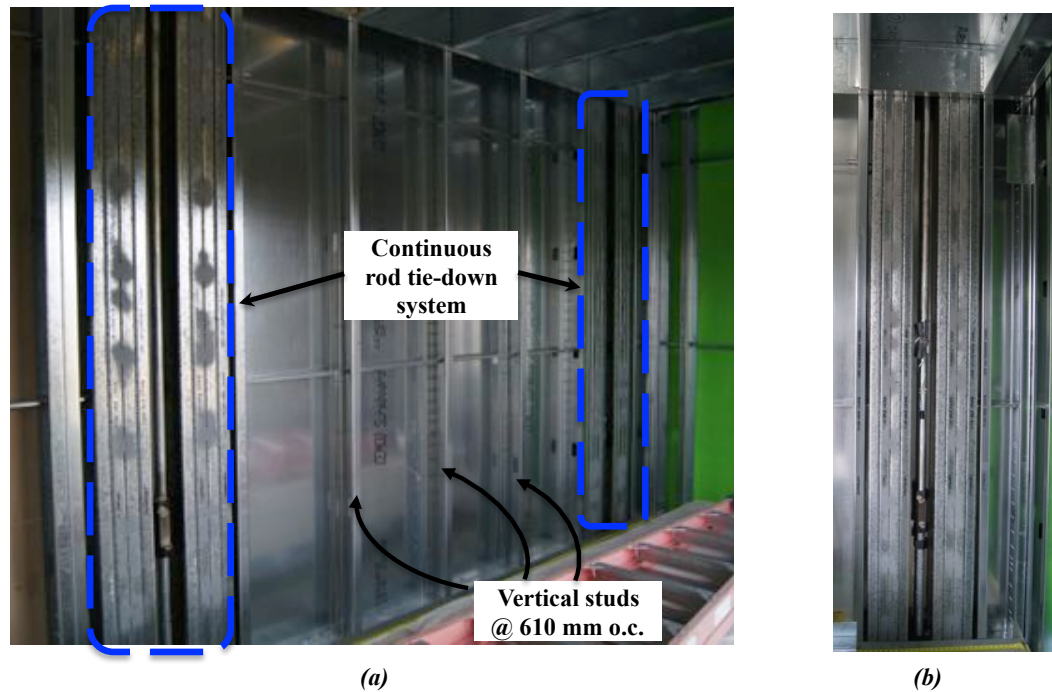


Figure 2.3. Corridor shear wall: (a) CFS framing (viewing from room side), and (b) tie-down assembly.

2.2.2 Gravity Walls

The gravity walls were located between the window openings at the building exterior as well as in the middle of the corridor between the shear walls at the two ends (Figure 2.2b). Since the gravity walls were designed to resist only vertical loads, they differed from the shear walls in two important aspects: 1) regular gypsum panels were used as the sheathing material on both sides of the framing, and 2) tie rods and compression posts were absent in the framing as these wall units are not intended to carry tension or compression induced via seismic loading (Figure 2.4). As a result, the shear strength of the gravity walls was significantly lower compared to the shear walls. The steel framing was constructed of 600S200-54 at 610 mm (24") o.c for intermediate studs and 600S200-68 for chord studs. In addition, both the top and bottom tracks were made of 600T200-54 (with the exception of the first-story bottom track that utilized

600T200-97). The gypsum panels were attached to framing by #8 drywall screws at a spacing of 152 mm (6") o.c. on boundary and 406 mm (16") o.c in field.

2.2.3 Floor Diaphragm

Supported on a ledger framing system, the floor and roof diaphragms were connected to the vertical structural system by attaching the diaphragm joists to the interior flange of the wall studs via a combination of rim-track and clip angle solution. The diaphragm joists were constructed of 1000S200-54 and the rim tracks constructed of 1000T200-54 at all floors of the building including the roof. The diaphragm was sheathed with composite structural panels on top of the joists. The composite panels were fabricated using fiber reinforced cement boards bonded with a layer of 0.838 mm (0.033") thick (20 ga.) sheet steel (the cement board thickness was 14 mm (9/16") at the second to the sixth floor and 11 mm (7/16") at the roof). In addition, the underside of the third floor and roof was sheathed with 16 mm (5/8") thick Type X gypsum panels to provide a compartmentalized fire-testing environment. Similarly, the gypsum panels to the joist and rim tracks using #8 drywall screws that were spaced at 152 mm (6") o.c both in field and on boundary.

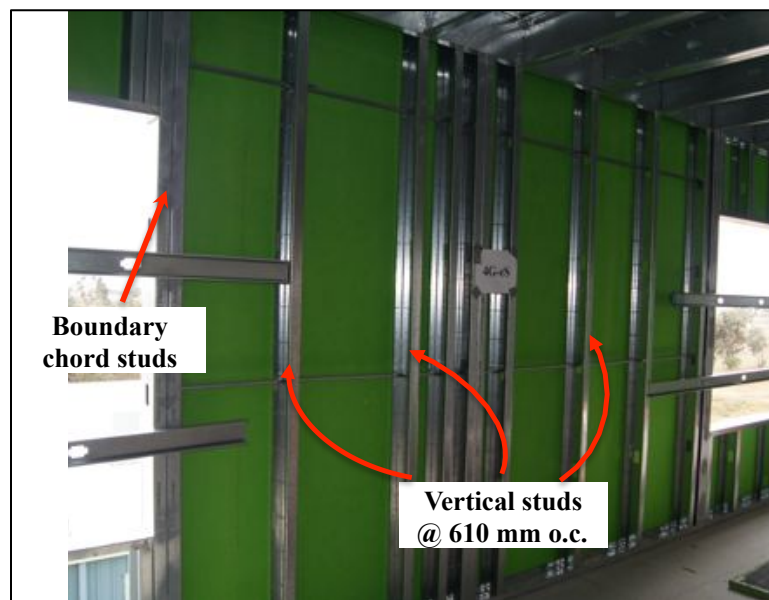


Figure 2.4. Exterior non-shear gravity wall CFS framing (view from building interior).

2.3 Nonstructural Systems

The test building incorporated three categories of nonstructural systems, namely, 1) interior partition walls, 2) doors, and 3) household appliances. Each nonstructural system is briefly described in the following subsections.

2.3.1 Partition Walls

As shown in Figure 2.2b, the test building consisted of two interior partition walls in the transverse direction of the building from level 2 to level 6 (~0.6 m (2 ft) west of the centerline). No partition walls were located at the first level due to insufficient attachment conditions to the shake table platen. As non-load bearing architectural components of the building, the partition walls compartmentalized the building interior into four separated rooms located at each corners. Each partition wall provided an opening to accommodate a door for accessing the room on the west side of the building.

The partition wall spanned from the lower floor to the underside of the upper floor diaphragm joists with a height of ~2.8 m (9'-2"). As shown in Figure 2.5a, the steel framing of all partition walls utilized 362VS125-33 at 610 mm (24") o.c for both intermediate studs and chord studs. The bottom tracks of all partition walls constructed using regular tracks 362T150-33, while the top tracks utilized slotted tracks 362CST250-33 with a slot length of 38 mm (1.5"). Partition wall sheathing utilized 16 mm (5/8") thick Type X gypsum panels that were attached to the framing on both sides using #8 drywall screws at a spacing of 152 mm (6") o.c. on boundary and 406 mm (16") o.c in field (Figure 2.5b).

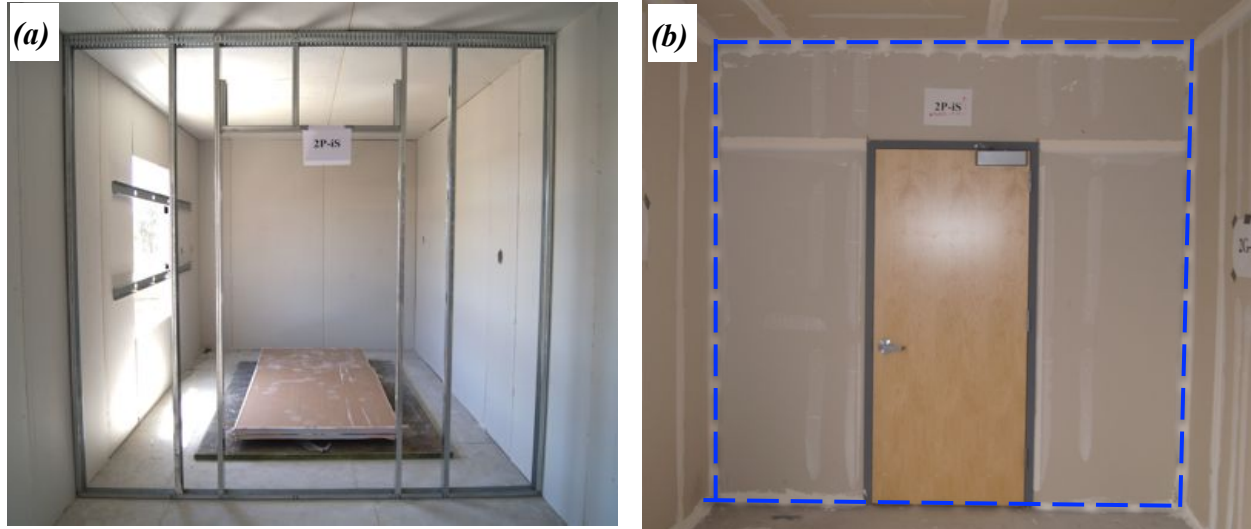


Figure 2.5. Interior partition wall: (a) CFS framing, and (b) finished wall.

2.3.2 Doors

As shown in Figure 2.6, the building was equipped with four doors at level 2 through level 6 and (two at the corridor and two on transverse partition walls). However, level 1 consisted of only two doors (at the corridor) due to the absence of interior partition walls. All the corridor doors on the walls and the south partition walls were single-swing doors (Figure 2.7a-b), each with an opening dimension of about 1.0 m (3'-6") in width and 2.2 m – 2.5 m (7'-3" – 8'-3") in height. In contrast, the doors on the north partition walls employed the form of double-swing door (Figure 2.7c), single-swing door with a side lite frame (Figure 2.7d), and sliding door with a side lite frame (Figure 2.7e), thus requiring an opening width twice as much as that of a single-swing door. In addition, it is noted that the doors at level 2 and 6 were fire-rated doors since these two levels were selected as fire test compartment. According to the NFPA 80 standards (NFPA, 2013), the doors at level 2 had a 60-minute fire rating and those at level 6 had a 20-minute fire rating. Detailed descriptions of all the door types, opening dimensions, and fire resistance ratings are summarized in Table 2.1.

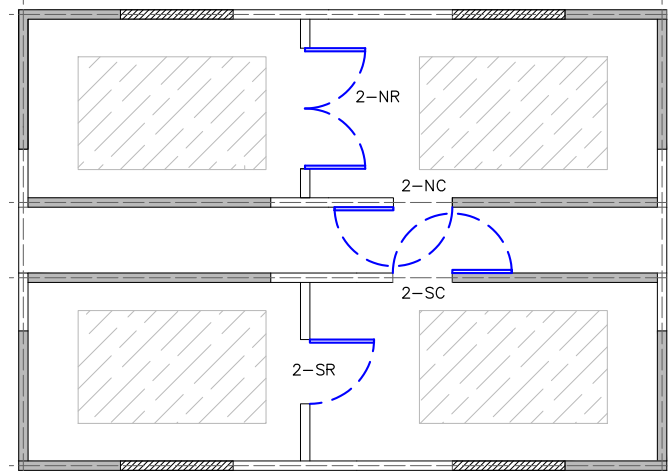


Figure 2.6. Plan layout of the doors (level 2, typical of levels 3-6).

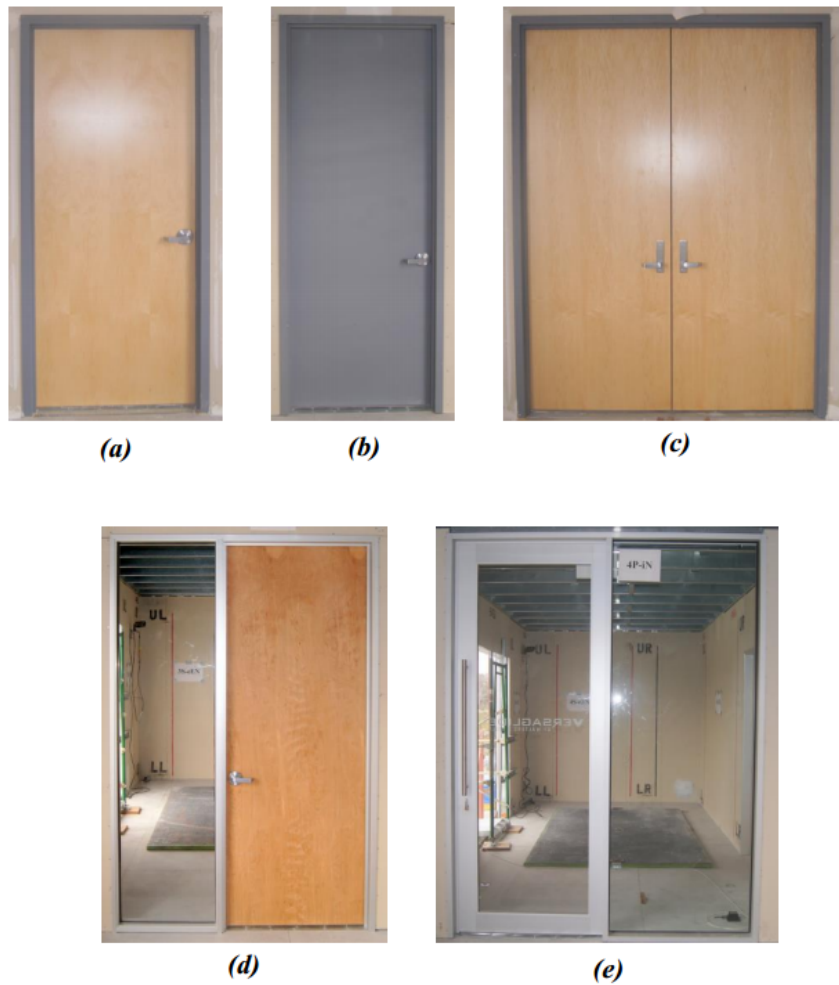


Figure 2.7. Photographs of the typical door types: (a) single-swing wood door (1.0 m × 2.2 m), (b) single-swing metal door with a 20-minute fire rating (1.0 m × 2.5 m), (c) double-swing wood door (2.0 m × 2.5 m) (d) single-swing wood door with a side lite frame (1.6 m × 2.5 m) (e) sliding door with a side lite frame (2.0 m × 2.7 m).

Table 2.1. Detailed descriptions of the doors.


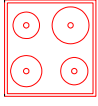
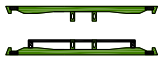

<i>Level</i>	<i>Short name¹</i>	<i>Description</i>	<i>Opening width and height (m x m)</i>	<i>Fire rating (min)</i>
1	1-NC	Single-swing wood door with an aluminum frame	1.0 x 2.5	N/A
	1-SC	Single-swing hollow metal door with a hollow metal frame	1.0 x 2.5	N/A
2	2-NR	Double-swing hollow metal door with a hollow metal frame	2.0 x 2.2	60
	2-NC	Single-swing wood door with an aluminum a frame	1.0 x 2.2	60
	2-SC	Single-swing wood door with a hollow metal frame	1.0 x 2.2	60
	2-SR	Single-swing wood door with a hollow metal frame	1.0 x 2.2	60
3	3-NR	Single-swing wood door with an aluminum side lite frame	1.6 x 2.1	N/A
	3-NC	Single-swing wood door (vision lite) with an aluminum frame	1.0 x 2.2	N/A
	3-SC	Single-swing hollow metal door (vision lite) with a hollow metal frame	1.0 x 2.2	N/A
	3-SR	Single-swing hollow metal door with a hollow metal frame	1.0 x 2.5	N/A
4	4-NR	Single-sliding hollow metal door (vision lite) with an aluminum side lite frame	2.0 x 2.7	N/A
	4-NC	Single-swing wood door with an aluminum frame	1.0 x 2.2	N/A
	4-SC	Single-swing wood door with a hollow metal frame	1.0 x 2.2	N/A
	4-SR	Single-swing wood door with a hollow metal frame	1.0 x 2.2	N/A
5	5-NR	Double-swing wood door with an aluminum frame	1.9 x 2.2	N/A
	5-NC	Single-swing wood door with a hollow metal frame.	1.0 x 2.2	N/A
	5-SC	Single-swing hollow metal door with a hollow metal frame	1.0 x 2.2	N/A
	5-SR	Single-swing hollow metal door with a hollow metal frame.	1.0 x 2.2	N/A
6	6-NR	Double-swing wood door with a hollow metal frame	2.0 x 2.5	20
	6-NC	Single-swing wood door (vision lite) with an aluminum frame	1.0 x 2.2	20
	6-SC	Single-swing hollow metal door (vision lite) with a hollow metal frame.	1.0 x 2.2	20
	6-SR	Single-swing hollow metal door with a hollow metal frame.	1.0 x 2.5	20

¹ 1-6 = level number; NC = north corridor; NR = north room; SC = south corridor; SR = south room.

2.3.3 Appliances

The test building featured a realistic household environment on levels 1 and level 6, which included common household appliances and fire safety devices. The purpose of incorporating these items in the test program was to assess the gas-related fire ignition potential of typical residential settings during an earthquake event. The appliances installed in the building included gas and electric ranges, water heaters, wall-mounted television sets, and safety devices such as seismic gas shutoff valves. A complete itemized list of the appliance and safety devices installed in the building are summarized in Table 2.2. This table also provides the associated geometric dimensions and weights of individual items.

Table 2.2. Appliances and their associated specifications.

<i>Appliance legend</i>	<i>Description</i>	<i>Dimensions (m)</i>	<i>Weight (kg)</i>
	Gas water heater (Make: Envirotamp)	0.50 (Dia.) \times 1.55 (H)	61.2 (empty) 213.3 (full)
	Electric water heater (Make: Whirlpool)	0.53 (Dia.) \times 1.26 (H)	40.8 (empty) 193.0 (full)
	Gas range (Make: Kenmore)	0.52 (D) \times 0.76 (W) \times 1.21 (H)	76.2
	Electric range (Make: Kenmore)	0.72 (D) \times 0.76 (W) \times 1.21 (H)	63.5
	HDTV (Make: RCA)	0.09 (D) \times 1.40 (W) \times 0.80 (H)	21.5
	HDTV (Make: Samsung)	0.09 (D) \times 1.37 (W) \times 0.80 (H)	23.0
	SGSV (Model 300)	0.10 (D) \times 0.12 (W) \times 0.10 (H)	0.9
	SGSV (Model AGV-75)	0.07 (D) \times 0.04 (W) \times 0.0 (H)	0.5

Notes: Dia. – diameter; D – depth; W – width; H – height.

Figure 2.8 illustrates the appliances and safety device plan layout at level 1 and level 6, respectively. The building was outfitted with two electric range units in the southwest compartment and two gas range units in the southeast compartment at each level. These units were placed on a $\sim 2.4 \text{ m} \times 2.4 \text{ m}$ (8 ft \times 8 ft) elevated wood-framed platform with resilient tile flooring (see Figure 2.9a). The two ranges in the same compartment were placed in a side-by-side configuration, one as an unrestrained unit and the other restrained at its base (Figure 2.9a). Furthermore, a total of six water heaters (three gas water heaters and three electric water heaters) were installed in north compartments at level 1 and level 6, respectively (Figure 2.9b). The four

braced water heaters each utilized a different bracing strategy to attach them to the adjacent wall framing (e.g., plumbers tape, off-the-shelf strap, and combined conduit and plumbers tape). With the exception of the one in the northwest compartment of level 6, all the remaining three water heaters were filled with water or sand to their respective operating weight capacity. In addition, two high-definition television sets were mounted on the corridor walls at level 1.

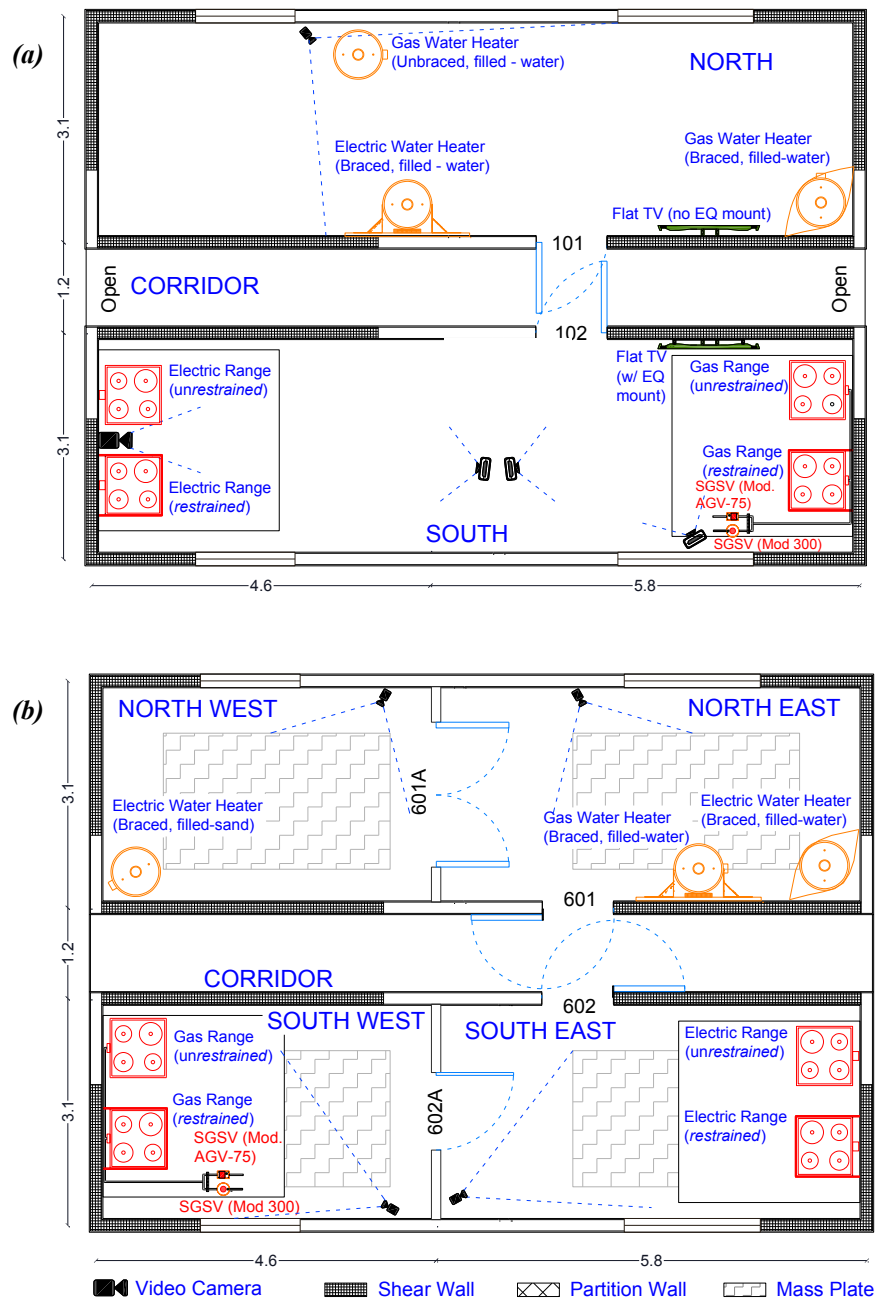


Figure 2.8. Appliance plan layout: (a) level 1, and (b) level 6 (note the hatched pattern on level 6 delineates the outline of the mass plates, and elevated wood-framed platform was placed over the mass plates).

Two gas piping assemblies were installed in the southeast compartment at level 1 and southwest compartment at level 6 (Figure 2.9c). Each assembly consisted of two different seismic gas shutoff valves connecting to flexible piping to a floor-mounted gas supply pipe, reflecting the typical installation conditions of residential construction. These safety devices were designed as emergency gas shutoff devices in the event of earthquakes, and therefore they were air-pressurized during all the seismic tests to simulate their functionality. It is also noted that a network of six video cameras was installed within these appliance compartments to monitor their seismic response during the earthquake tests.

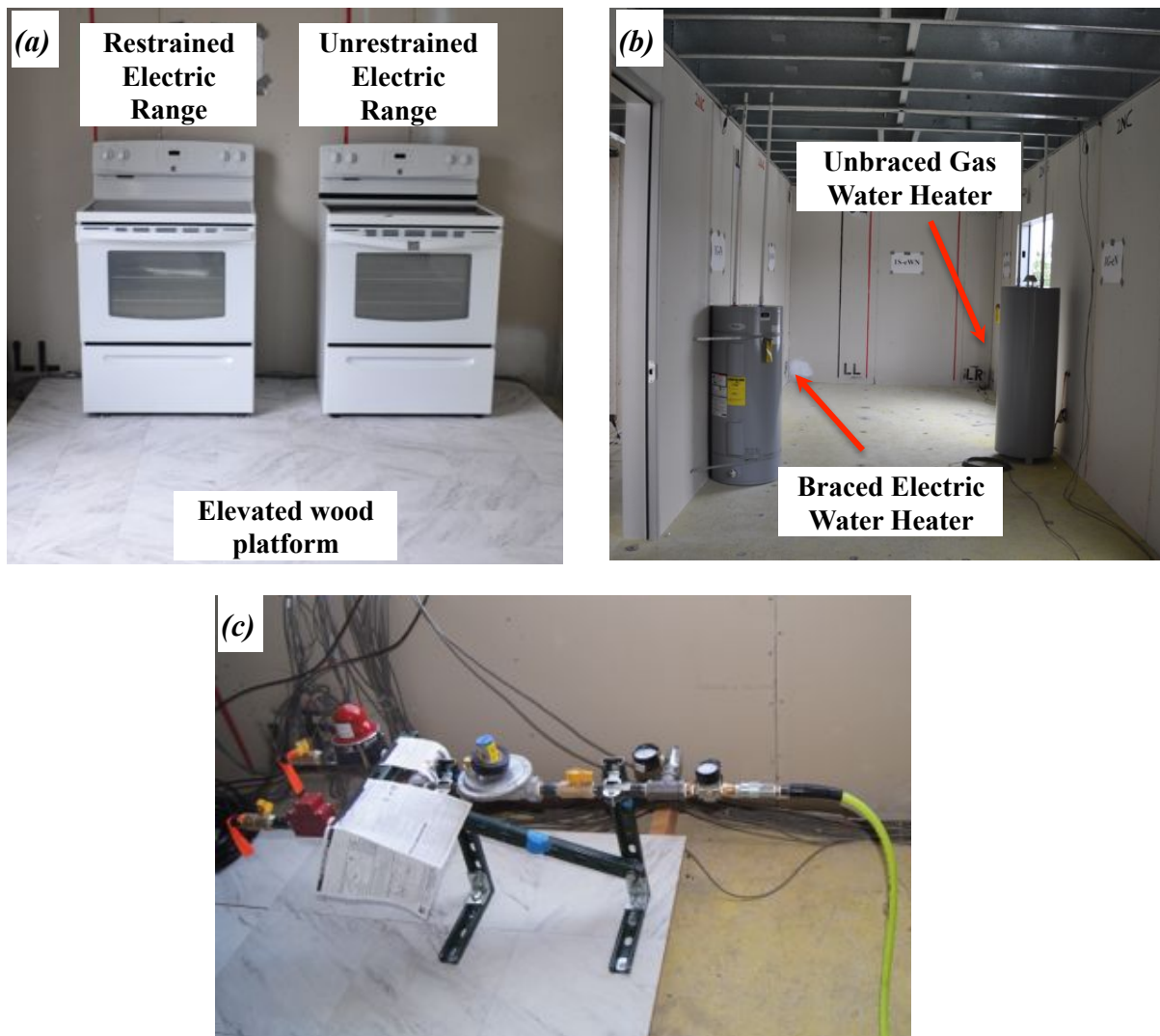


Figure 2.9. Photographs of appliances at level 1: (a) electric range units, (b) water heaters, and (c) gas piping assembly with seismic gas shutoff valves.

2.4 Building Construction

With the exception of the structural wall system at the first level, the building structural skeleton (i.e., wall and floor systems) was constructed using prefabricated panels. The building diaphragm at each floor consisted of six prefabricated segments (two for the corridor and one each for the four rooms). Figure 2.10 illustrates the layout of the diaphragm penalization pattern as well as the prefabricated diaphragm segments. It is noted that the segments at the east end were about 1.2 m (4 ft) longer than their counterparts at the west end, and therefore the transverse boundary lines for the east and west panels were 0.6 m (2 ft) west of the building centerlines. As shown in Figure 2.11, the structural wall system (shear walls and gravity walls) at each level consisted of twelve prefabricated panels (eight longitudinal wall panels and four transverse wall panels). Figure 2.11 also illustrates the elevation of an exterior wall panel and a corridor wall panel at the construction stage.

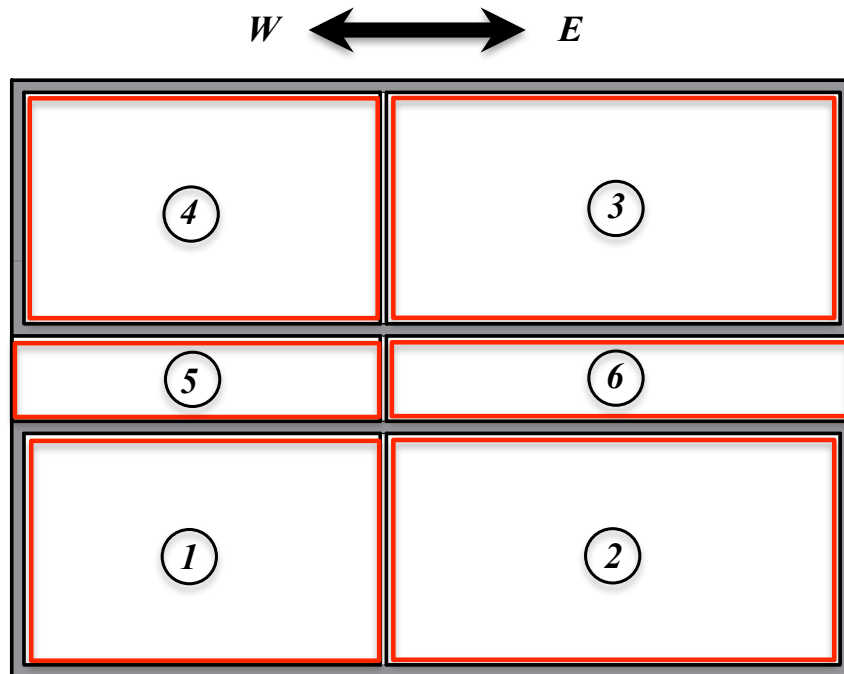


Figure 2.10. Diaphragm panel pattern (top) and photographs of the prefabricated diaphragm segments prior to installation (bottom) (room segments #1 – #4 and corridor segments #5 and #6).

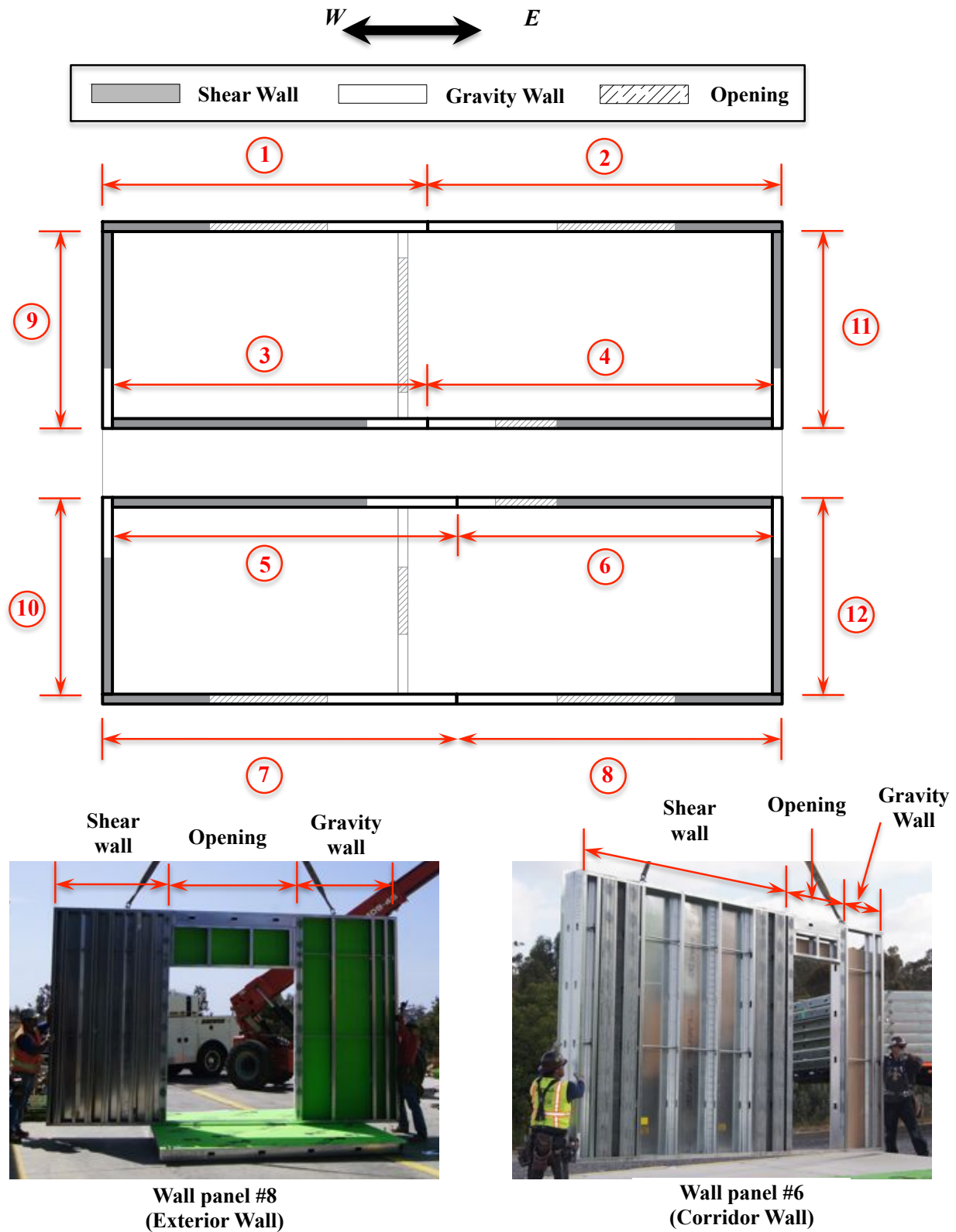


Figure 2.11. Prefabricated wall panel pattern (top) and sample photographs of prefabricated wall segments (bottom).

Construction of the test building commenced on April 15, 2016 with the shake table platen tie-down system installation. A total of 80 large-diameter rods were used to attach the first-level bottom tracks to the table at a space at 0.6 m (2 ft) along almost all the tracks (Figure 2.12a). Subsequently, the first-story wall system was fabricated in-situ for a total of four days (Figure 2.12b). Following completion of the first-story wall system, the building construction significantly expedited as a result of highly efficient panelized construction (Figure 2.12c). The construction of the upper levels progressed at a rate of one level per day. The erection of the building skeleton was completed on April 27, 2016 (within a total of nine days) (Figure 2.12d). Figure 2.12e shows the layout of the mass plates (one at each quadrant) at the roof of the building, which represented the typical mass configuration of the roof and all other floors during the earthquake tests. These plates were installed on and anchored to the floor diaphragms in conjunction with building erection.

Interior construction commenced immediately following the completion of the building erection. Activities related to interior construction included: 1) in-situ installation of interior partition framing, 2) interior installation of gypsum panels (structural walls, nonstructural walls, and ceiling), 3) door installation, and 4) appliance installation (on the first and sixth floors). These activities spanned about an entire month and the interior installation was completed at the beginning of June 2016. The building demolition began on July 11, 2016 (a week following the completion of all tests) and finished on July 20, 2016. Interested readers are referred to the video links^{1,2} of the building construction and demolition time lapses.

In conjunction with building erection, a temporary platform stair tower was installed on the northeast side of the building to support floor-to-floor access to the test building. The stair tower was detached during all earthquake tests, however, provided full access to the building at all floors including the roof throughout the interior construction and following each test during inspection phases.

¹ Construction time lapse available at https://www.youtube.com/watch?v=IFq7Nv_020c.

² Demolition time lapse available at <https://www.youtube.com/watch?v=ElOiksCJUKM>.



Figure 2.12. Construction of the test building: (a) building tie-down system (photo taken on April 16, 2016), (b) in-situ installation of first-story wall system (photo taken on April 19, 2016), (c) installation of a prefabricated wall panel at the third story (photo taken on April 23, 2016), (d) completion of building skeleton erection (hoisting the last piece of roof panel) (photo taken on April 27, 2016), and (e) roof mass plate layout prior to the earthquake tests (photo taken on June 10, 2016).

3 TEST PROTOCOL

The test program consisted of a three-week sequence of nine earthquake and six fire tests between June 13 and July 1, 2016. During the first week, the building was subjected to seven earthquakes with increasing input motion intensity on three days. Subsequently, live fire tests were conducted on the earthquake-damaged building at the second and sixth levels during a period of three days. The test program concluded with two post-fire earthquake tests on the final test day at the end of the third week of testing. To complement the earthquake and fire test sequence, low-amplitude, ambient vibration tests in the form of white noise and tire (shock) tests were conducted throughout the construction and the testing phase. It is noted that all the earthquake and white noise test motions were applied in the east-west direction using the single-axis shake table, whose axis coincided with the longitudinal axis of the building.

3.1 Pre-test Vibration Test Protocol

Low-amplitude vibration tests were conducted on three days during the building construction. These vibration tests were intended to identify the pre-test dynamic characteristics of the building at the various stages during the construction. As summarized in Table 3.1, the building had five different configurations during with varied roof mass plate layout and the building interior installation aspects (e.g., interior gypsum attachment conditions, interior partition installation, and doors in opened and closed configurations). The vibration tests included pulse (with a targeted peak acceleration of 0.08 g) and banded (0.25-25 Hz) white noise base excitations applied on the building using the LHPOST. As shown in Table 3.2, white noise tests consisted of input excitations of two distinct amplitude levels with root-mean-square (RMS) accelerations of 1.5% g and 3.0% for each configuration (a white noise test with 5.0% g RMS amplitude was conducted only while the building was at configuration C1). It is noted that shock tests were conducted on the second test day of the construction phase by impacting the building roof in different directions. In addition, ambient vibration data were collected during the construction and the testing phase (between May 5 and July 1, 2016) to capture the evolution of the building dynamic characteristics.

Table 3.1. Low-amplitude vibration test sequence during construction phase

<i>Date</i>	<i>Type of tests</i>	<i>Building configuration</i>
May 5, 2016	Pulse White noise	C1 : roof mass plates in layout 1 (asymmetric) ¹ ; fully attached interior gypsum; partition wall installation partially completed; doors not installed
May 16, 2016	Pulse White noise Shock	C2 : roof mass plates in layout 2 (asymmetric) ² ; minimally attached interior gypsum; partition wall installation partially completed; doors partially installed C3 : roof mass plates in symmetric layout (baseline) ³ ; minimally attached interior gypsum; partition wall installation partially completed; doors partially installed
June 9, 2016	Pulse White noise	C4 : roof mass plates in symmetric (baseline) layout; fully attached interior gypsum; partition wall installation completed; all doors open C5 : roof mass plates in symmetric (baseline) layout; fully attached interior gypsum; partition wall installation completed; all doors closed

¹ mass plate layout 1 – two plates each at the northeast and southwest quadrants (asymmetric);

² mass plate layout 2 – two plates each at the northeast and northwest quadrants (asymmetric);

³ symmetric (baseline) layout – one plate each at the four quadrants (symmetric).

Table 3.2. White noise test sequence and the building configuration

<i>Date</i>	<i>Test</i> ¹	<i>Short name</i>	<i>Configuration</i>
May 5, 2016	1.5% g RMS WN (4 min)	WNC:1A	C1
	3.0% g RMS WN (4 min)	WNC:1B	
	5.0% g RMS WN (4 min)	WNC:1C	
May 16, 2016	1.5% g RMS WN (3 min)	WNC:2A	C2
	3.0% g RMS WN (3 min)	WNC:2B	
	1.5% g RMS WN (3 min)	WNC:3A	C3
	3.0% g RMS WN (3 min)	WNC:3B	
June 9, 2016	1.5% g RMS WN (3 min)	WNC:4A	C4
	3.0% g RMS WN (3 min)	WNC:4B	
	1.5% g RMS WN (3 min)	WNC:5A	C5
	3.0% g RMS WN (3 min)	WNC:5B	

RMS = root mean square; WN = white noise test.

3.2 Earthquake Test Protocol

The test building was subjected to a sequence of seven earthquake motions prior to and two motions following the fire tests (Table 3.3). The input earthquake motions adopted in for the shake table testing were selected from four historical earthquake records, namely: Rio Dell Overpass from the 1992 Cape Mendocino earthquake, Canoga Park and Rinaldi Receiving Station both from the 1994 Northridge earthquake, and Curico from the 2010 Maule earthquake in Chile. With the exception of the Curico motion that was recorded from a long-duration subduction earthquake in Chile, the remaining three motions were recorded from strong earthquakes that occurred in California in the past few decades. Each input motion was amplitude-scaled to its targeted intensity level, which was defined as the spectral acceleration averaged between half and one and a half times the building fundamental period associated with the longitudinal vibration (in the direction of shaking). It is noted that spectral matching was not performed on the motions, in an effort to preserve the frequency content of the original recorded motions. As shown in Table 3.4, low-amplitude vibration base excitation tests were conducted before and after each earthquake test for identifying the building dynamic characteristics at different stages of the testing phase.

Table 3.3. Seismic test protocol

<i>Date</i>	<i>Station – Earthquake (Performance target)</i>	<i>Short Name</i>
June 13, 2016 (Test day 1)	Rio Dell Overpass – 1992 Cape Mendocino (service level)	EQ1:RIO-25
	Canoga Park – 1994 Northridge (service level)	EQ2:CNP-25
	Curico – 2010 Maule, Chile (service level)	EQ3:CUR-25
June 15, 2016 (Test Day 2)	Canoga Park – 1994 Northridge (service level)	EQ4:CUR-25
	Canoga Park – 1994 Northridge (50% design level)	EQ5:CNP-50
	Canoga Park – 1994 Northridge (design level)	EQ6:CNP-100
June 17, 2016 (Test Day 3)	Canoga Park – 1994 Northridge (MCE level)	EQ7:CNP-150
Fire test phase (June 27-29, 2016)		
July 1, 2016 (Test Day 4 – post- fire earthquake tests)	Rio Dell Overpass – 1992 Cape Mendocino (service level)	EQ8:RIO-25
	Rinaldi Receiving Station– 1994 Northridge (MCE level)	EQ9:RRS-150

Table 3.4. White noise test sequence and the associated building states

Date	Dynamic Test	Test Name	Building State	Inspection
June 13, 2016	1.5% g RMS WN	WN _E :0A	S0	Pre-EQ1
	3.0% g RMS WN	WN _E :0B		
	EQ1:RIO-25 (service level motion)			
	1.5% g RMS WN	WN _E :1A	S1	
	EQ2:CNP-25 (service level motion)			
	1.5% g RMS WN	WN _E :2A	S2	Partial
	EQ3:CUR-25 (service level motion)			
	1.5% g RMS WN	WN _E :3A	S3	
	3.0% g RMS WN	WN _E :3B	S3	Post-EQ3
June 15, 2016	1.5% g RMS WN	WN _E :3C	S3	
	3.0% g RMS WN	WN _E :3D	S3	
	EQ4:CNP-25 (service level motion)			
	1.5% g RMS WN	WN _E :4A	S4	—
	3.0% g RMS WN	WN _E :4B	S4	Partial
	EQ5:CNP-50 (50% design level motion)			
	1.5% g RMS WN	WN _E :5A	S5	—
	3.0% g RMS WN	WN _E :5B	S5	
	EQ6:CNP-100 (design level motion)			
	1.5% g RMS WN	WN _E :6A	S6	—
	3.0% g RMS WN	WN _E :6B	S6	Post-EQ6
June 17, 2016	1.5% g RMS WN	WN _E :6C	S6	—
	3.0% g RMS WN	WN _E :6D	S6	
	EQ7:CNP-150 (MCE level motion)			
	1.5% g RMS WN	WN _E :7A	S7	—
	3.0% g RMS WN	WN _E :7B	S7	Post-EQ7
Fire test phase (June 27-29, 2016)				
July 1, 2016	1.5% g RMS WN	WN _E :8A	S8	Pre-EQ8
	3.0% g RMS WN	WN _E : 8B	S8	
	EQ8:RIO-25 (service level aftershock)			
	1.5% g RMS WN	WN _E :9A	S9	—
	3.0% g RMS WN	WN _E :9B	S9	Partial
	EQ9:RRS-150 (Post-EQ9)			

Notes: RMS = root mean square; WN = white noise test; EQ = earthquake test.

Figures 3.1 and 3.2 present the acceleration time histories of the achieved input earthquake motions. The 5% damped elastic response spectra of the achieved motions are shown in Figure 3.3. The maximum peak acceleration, velocity, displacement, spectral acceleration at building fundamental period, and strong motion duration of each achieved input motion are also summarized in Table 3.5. It is noted that the strong motion duration of all input motions were between 10 and 20 seconds, with the exception of the subduction event (EQ3) that had a strong duration of over 50 seconds. It is also clearly indicated in the table that the first seven earthquake motions (pre-fire test sequence) were applied with increasing intensity to progressively damage the building, as the peak input accelerations of the motions increase from around 0.15 g to 0.9 g and the fundamental period spectral accelerations increased from 0.3 g to 2.0 g. The last two test motions (post-fire test sequence) were intended to represent a service-level aftershock event (EQ8 – a replicate of the first input motion EQ1) and a near-fault extreme earthquake event (EQ9) with a peak input acceleration above 1.0 g.

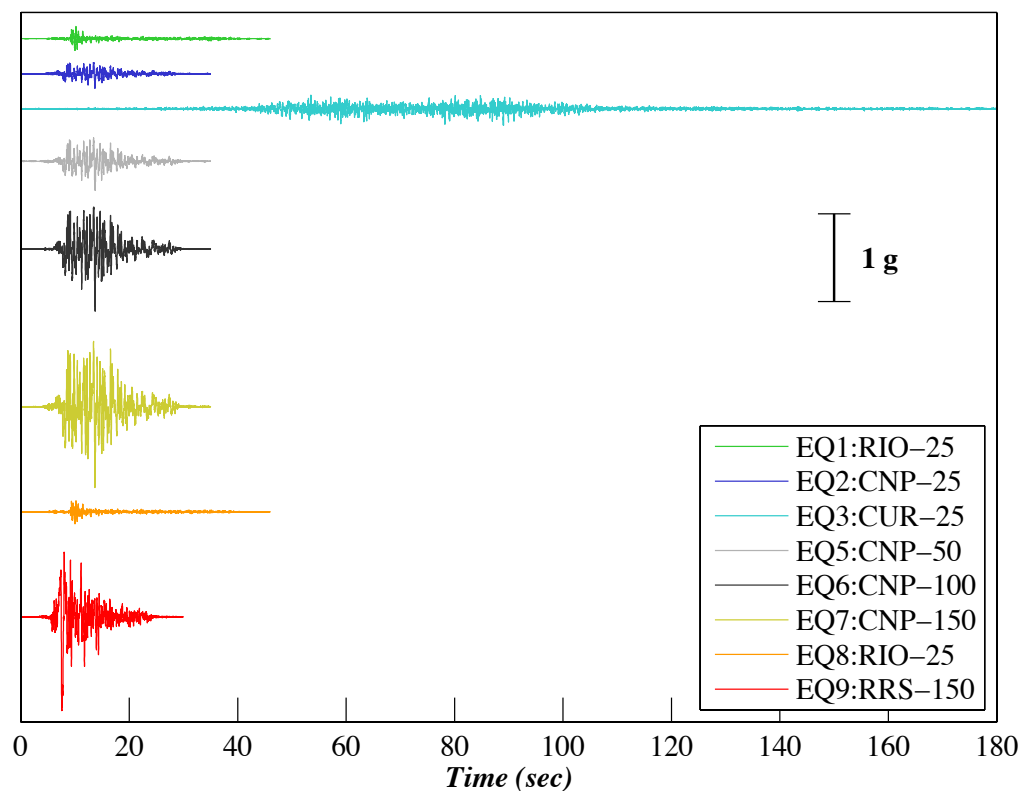


Figure 3.1. Acceleration time histories of achieved input motions.

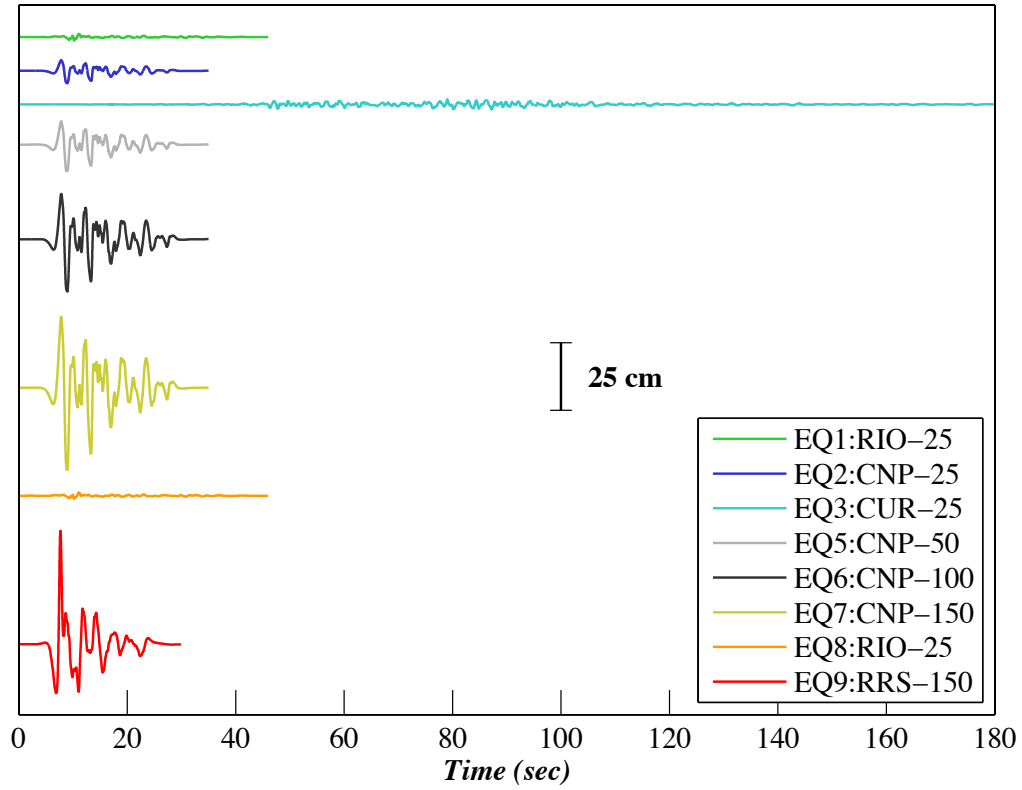


Figure 3.2. Displacement time histories of achieved input motions.

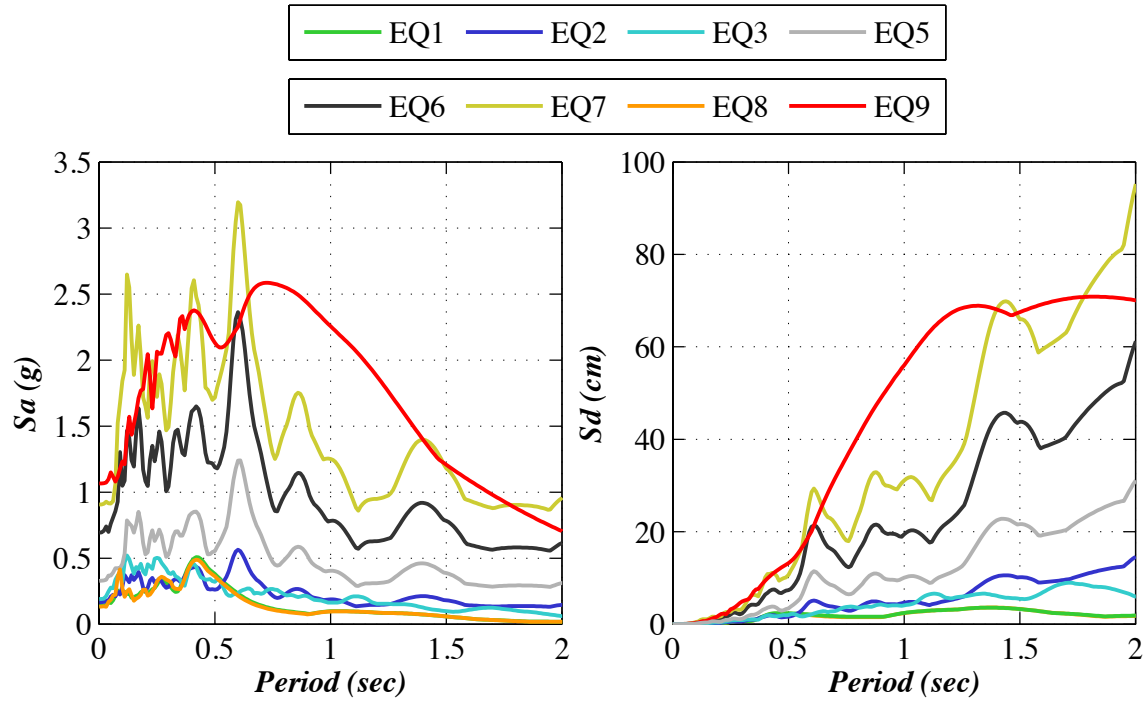


Figure 3.3. Elastic response spectra of achieved motions ($\xi = 5\%$): (a) pseudo-acceleration spectra, and (b) displacement spectra.

Table 3.5. Summary of select characteristics of achieved earthquake input motions

<i>Test Motion</i>	<i>PIA (g)</i>	<i>PIV (cm/s)</i>	<i>PID (cm)</i>	<i>Sa(T₁,5%) (g)</i>	<i>D_{s,5-95} (sec)</i>
EQ1:RIO-25	0.14	10.98	1.29	0.28	20.1
EQ2:CNP-25	0.17	22.14	4.68	0.32	11.4
EQ3:CUR-25	0.19	11.39	1.90	0.34	53.7
EQ4:CNP-25	0.17	23.41	5.00	0.35	11.9
EQ5:CNP-50	0.33	45.96	10.05	0.67	11.1
EQ6:CNP-100	0.69	90.61	19.77	1.37	10.4
EQ7:CNP-150	0.91	131.90	31.00	2.01	11.2
EQ8:RIO-25	0.13	10.30	1.20	0.09	16.7
EQ9:RRS-150	1.07	176.20	42.60	2.54	7.2

PIA – peak input acceleration; PIV – peak input velocity; PID – peak input displacement; Sa(T₁,5%) – elastic spectral acceleration of the input motion (T₁ represents the fundamental period of the building in the direction of shaking); D_{s,5-95} – strong motion duration.

3.3 Fire Test Protocol

Following the completion of earthquake tests EQ1-EQ7, the building was subjected to six compartment fire tests on three consecutive days at level 2 (four tests) and level 6 (two tests). The fire test compartments at these two levels represented a 60-minute fire resistance rating construction in the undamaged condition. It is noted, however, that the pre-fire earthquake tests induced varying levels of drywall damage to the test compartments at the two levels, as a result of variation in seismic drift demands at the two floors. Gypsum drywall damage at level 2 occurred in the form of crushed and gapped panel joints as the drift demands exceeded 1% during the pre-fire earthquake test sequence, while the damage at level 6 was observed as minor (joint tape cracks and incipient corner crushing) due to the insignificantly small drift demands.

Table 3.6 summarizes the compartment fire test protocol, and the test sequence and the locations of individual tests are illustrated in Figure 3.4. Figure 3.5 provides three-dimensional schematics for all the fire test compartments. It is noted that the same amount of fuel (84 liters) for all fire tests with an expected fire size of 2.16 megawatt. The major variables considered in these fire tests were the compartment space and ventilation characteristics, as well as pre-fire

seismic damage. In addition, the atmospheric conditions during each test may also significantly affect the actual burn duration and fire size of individual tests.

Table 3.6. Fire test protocol

Test Date	Test #	Test Name	Location	Fire Characteristics
June 27 th , 2016 (Fire Test Day 1)	1	L2-SW-T1	Southwest compartment at level 2	Fuel: n-Heptane Quantity: 12 liters / pan No. of Pans: 6 Expected Heat release rate: 2.16 Megawatt
	2	L2-SE-T2	Southeast compartment at level 2	
June 28 th , 2016 (Fire Test Day 2)	3	L2-NW-T3	Northwest compartment at level 2	
	4	L2-C-T4	Corridor at level 2	
June 29 th , 2016 (Fire Test Day 3)	5	L6-C-T5	Corridor at level 6	
	6	L6-C-T6	Southwest compartment at level 2	

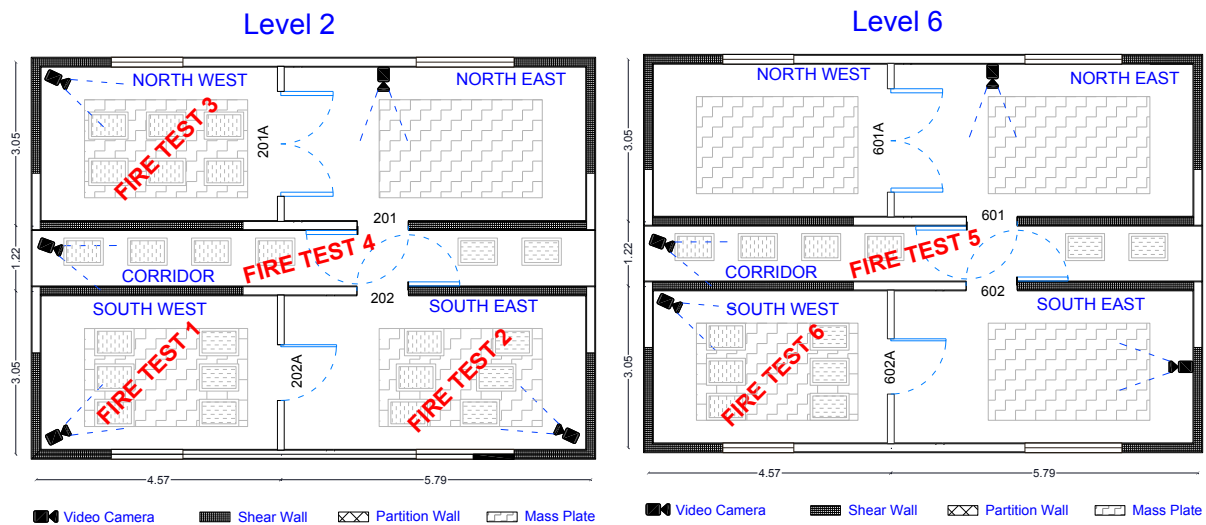


Figure 3.4. Fire test sequence specified on the building plan layout (level 2 and level 6).

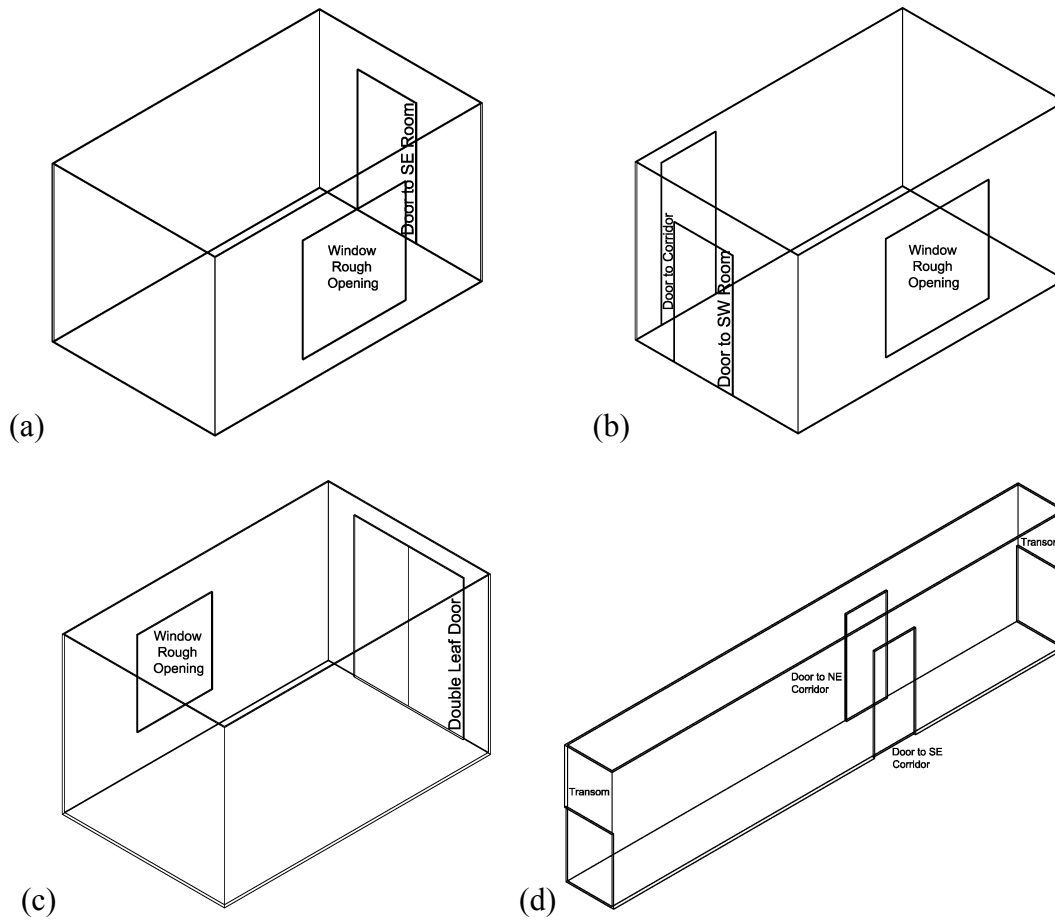


Figure 3.5. Three-dimensional view of the fire compartments: (a) southwest compartment, (b) southeast compartment, (c) northwest compartment, and (d) corridor.

4 MONITORING SYSTEM

4.1 Earthquake Phase

The performance of the test building was documented with four types of monitoring systems throughout the shake table test phase. These systems included still cameras, video cameras, analog sensors, and a global positioning system (GPS). A description of the important aspects of each of the four monitoring systems is provided in the following sections.

Analog sensors

During the shake table test program, the response of the test building was monitored with a dense analog sensor array consisting of 256 channels. The sensors consisted of accelerometers, displacement transducers (string potentiometers and linear potentiometers), and strain gauges. Table 4.1 provides a summary of different types of sensors on the test building and the corresponding measured responses. Figure 4.1 illustrates the plan layout of accelerometers installed at the second floor of the building. With the exception of the Kinometrics (high-resolution) accelerometer array that collected data using a standalone data acquisition system with a sampling frequency of 200 Hz, all remaining analog sensor channels were connected to a multi-node distributed data acquisition system with a 240 Hz sampling frequency. It is noted that some analogue sensors that were removed prior to the fire tests were not reinstalled due to insufficient installation conditions following the fire-induced damage to the building components (e.g., displacement transducers at level 2). Therefore, the number of sensors reduced slightly during the post-fire earthquake tests.

Table 4.1. Analog sensor instrumentation plan during the earthquake tests

<i>Sensor type</i>	<i>Count¹</i>	<i>Description of sensors</i>
Accelerometer (MEMS)	67 (57)	Floor accelerations at four corners and two ends of the corridors on all floors
Accelerometer (Kinometrics)	12 (0)	Floor accelerations at floor 2, 4, 6, and roof
String potentiometer	71 (52)	Shear distortions of individual shear walls and floor displacements
Linear potentiometer	39 (26)	Uplifting at ends of individual shear walls and relative displacement of floor joints
Strain gage	67 (59)	Tension rod strains

¹ Numbers in parenthesis denote count during the post-fire earthquake tests.

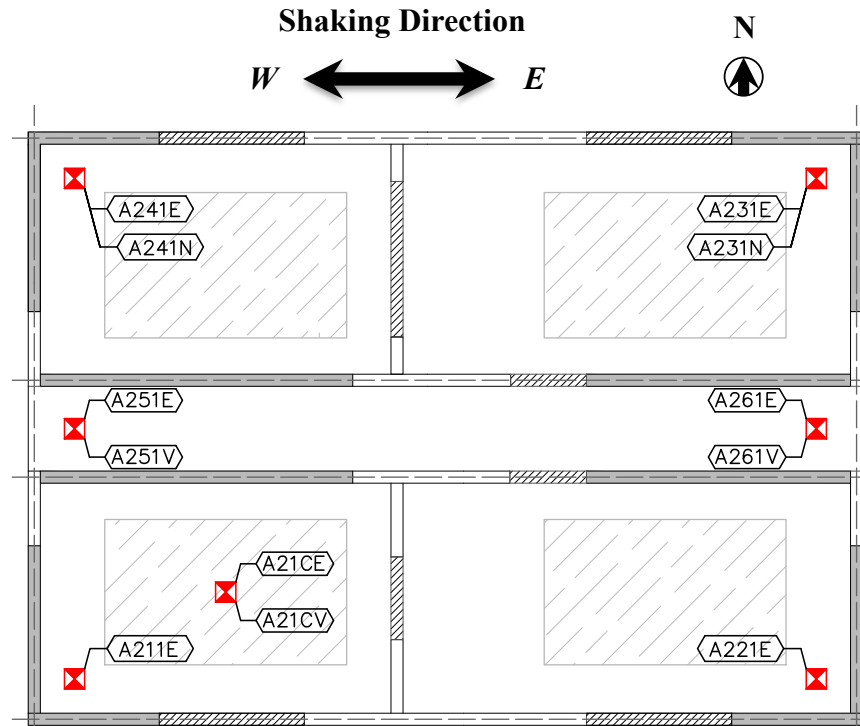


Figure 4.1. Plan layout of accelerometers on the second floor.

Video cameras

To complement data recorded from analog sensors, a large video camera system was developed to visually monitor the building interior and exterior during the shake table tests. The system consisted of more than 40 video cameras using four different types of cameras during the pre-fire earthquake test sequence. Table 4.2 provides a summary of the video camera system as installed on the test building. Figure 4.2 illustrates the building interior camera plan layout at the lower two levels.

Table 4.2. Video camera system during the earthquake tests

<i>Camera Type</i>	<i>Count¹</i>	<i>Camera View</i>
GoPro	14 (14)	Interior views of structural components and contents on the lower two levels
Coax	28 (8)	Interior views of structural components and contents on level 3 through the roof
IP	2 (2)	Exterior building views
Handy Cam	4 (3)	Exterior building views

¹ Numbers in parenthesis denote count during the post-fire earthquake tests.

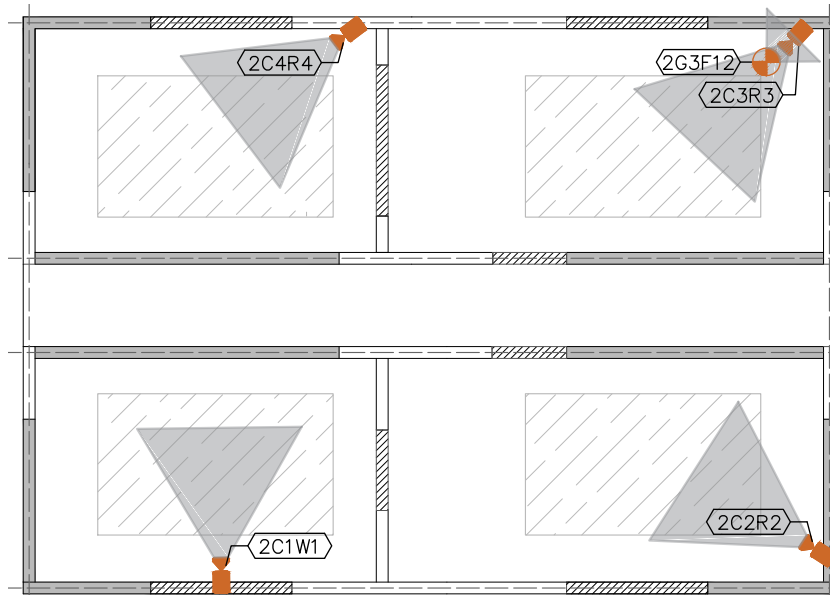
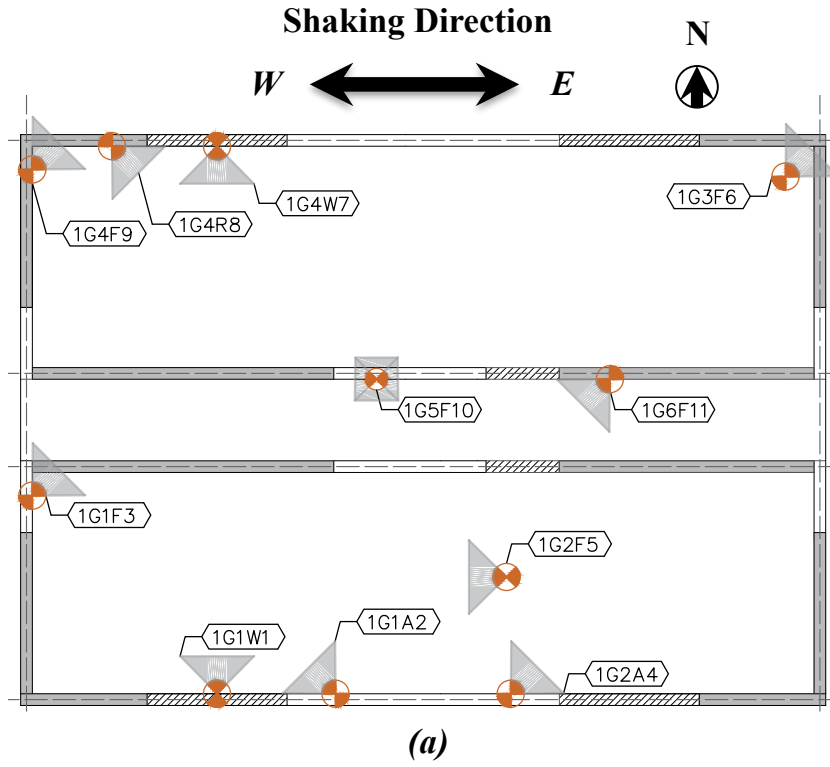


Figure 4.2. Plan layout of video cameras: (a) level 1, and (b) level 2.

Global positioning system (GPS)

The GPS installation and data acquisition was a collaborative effort between the project team and the researchers from Scripps Institute of Oceanography at UCSD. During the earthquake tests, five GPS stations were deployed at different locations of the test building: (a) three stations on the roof, namely, at the southwest and northwest corners as well as the approximate center of the roof, and (b) one station each at the west end of the corridor on the third and fifth floors. In addition, one static ground reference station was placed approximately 50 m to the west of the building (off the shake table). Direct displacements of the test building were measured by the GPS at a sampling frequency of 10 Hz. Additional information regarding the GPS system is available in Goldberg and Bock (2016).

Still cameras

Photographs were taken in the construction and the shake test phases by the project research team and industrial partners. These photographs were used to document (a) the construction progress as well as the as-built details of the structural components (e.g., shear wall framing, floor joists), and (b) the physical damage of the building at various stages during the test phase.

4.2 Fire Test Phase

During the fire test phase, a mobile data acquisition system was deployed on the test building to collect fire test data. The system was placed on the floor below the fire compartment floor for each test. The instrumentation consisted of two major types of sensing systems: (1) analog sensors (thermocouples) to measure the temperature response at various locations inside and outside of the fire test compartment, and (2) an array of video cameras deployed in the building interior and exterior to visually capture flame extension, leakage, and smoke propagation.

Temperature sensors

To measure the temperature response of the fire compartments and adjacent space during the fire tests, the test building was instrumented with a total of 233 thermocouples (Type K thermocouples with 24 gauge wires) in two major forms: a) 9 thermocouple trees (each consisting of 6 thermocouples), and (b) 186 individual thermocouples. Note that some

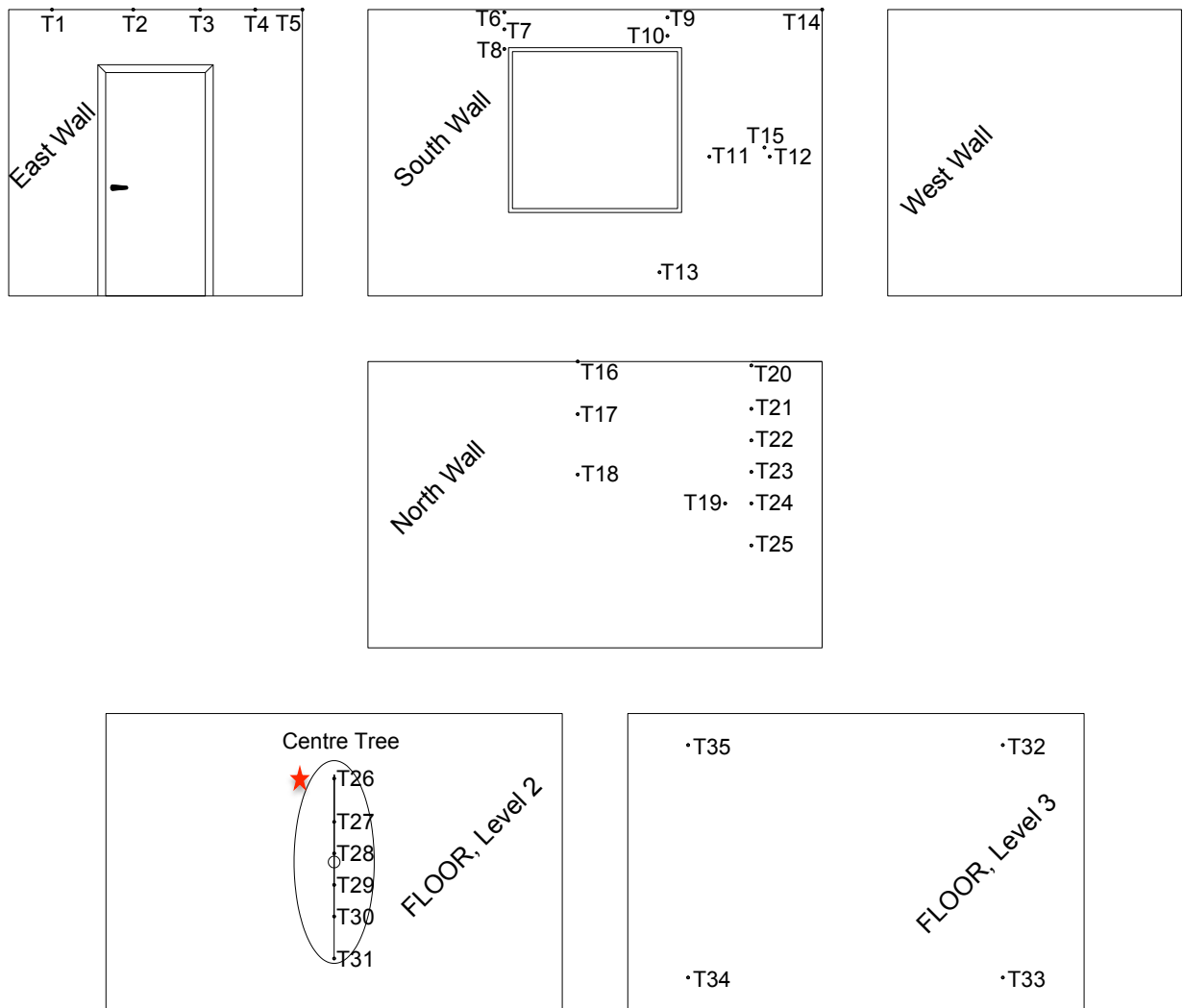
thermocouples were common for multiple tests. During individual fire tests, the temperature data were recorded for a minimum of one hour from ignition at a sampling frequency of 1 Hz.

- *Thermocouple trees* were configured by vertically placing the thermocouples on a threaded rod at the desired locations along the height. The rod was then mounted to the ceiling joist flange using #8 drywall screws. The thermocouple trees were fire-protected by wrapping 3 mm thick ceramic blankets on the threaded rods. The purpose of thermocouple trees was to measure the compartment temperature profiles along the vertical direction.
- *Individual thermocouples* were deployed all over the compartments at the locations of interest. The locations were decided at the completion of the pre-fire earthquake test sequence when drywall cracks and gaps were fully developed. The thermocouples were intended to measure the temperature propagation in the cracks. Data collected by individual thermocouples were used for understanding the temperature build-up inside of stud cavities, joist cavities, and door frames. Excessive temperatures at these locations may compromise the strength and stiffness of the structural framing and jeopardize the structural stability of light-gauge framing systems.

Table 4.3 summarizes the thermocouple instrumentation plan associated with each fire test. As shown in the table, the four fire tests conducted at level 2 included a larger amount of thermocouples compared to the two tests at level 6. Since the building sustained more severe damage to the interior gypsum drywalls at level 2, it required that more thermocouples be placed along the cracks or inside of the gaps. In addition, the thermocouple layout associated with Fire Tests 1 and 4 are schematically shown in Figures 4.3 and 4.4, respectively, since the temperature response measured during these two fire tests are discussed later in Chapter 5.

Table 4.3. Summary of thermocouple instrumentation plan.

Fire Test	Compartment	TC ID	Number	Location
1	South West Compartment, Level 2	T1 - T5	5	Fire Stop
		T6 - T10	5	Joint Crack (Window)
		T11 - T13, T15, T19	5	Stud Cavity
		T14, T32 - T35	5	Joist Cavity
		T16 - T18	3	Joint Crack (Wall)
		T20 - T25	6	TC Tree - Crack
		T26 - T31	6	TC Tree - Center
2	South East Compartment, Level 2	T1 - T5	5	Fire Stop
		T6, T18 - T20, T24, T42-T44	8	Joint Crack (Wall)
		T7 - T11, T14, T15	7	Joint Crack (Door)
		T27, T28, T30, T32-T34	6	Joint Crack (Window)
		T12, T13, T16	3	Door Frame Cavity
		T17, T21-T23, T25, T26	6	Stud Cavity
		T29, T31, T35	3	Stud Cavity (Window)
		T51 - T54	4	Joist Cavity
		T36 - T41	6	TC Tree - Crack
		T45 - T50	6	TC Tree - Center
3	North West Compartment, Level 2	T1-T3, T11	4	Joint Crack (Wall)
		T13, T16, T17	3	Stud Cavity
		T10, T14, T18, T25-T28	7	Joist Cavity
		T12, T15	2	Stud Cavity (Window)
		T4-T9	6	TC Tree - Crack
		T19 - T24	6	TC Tree - Center
4	Corridor, Level 2	T7-T9, T16-T21, T34-T37, T42-T56	28	Joint Crack (Wall)
		T10-T15, T38-T41, T57 - T64	18	Joint Crack (Door)
		T65-T68	4	Joist Cavity
		T22-T27	6	TC Tree - Crack
		T1-T6, T28-T33	12	TC Tree - Center
5	South West Compartment, level 6	T13, T26 (SE)	2	Joist Cavity
		T7-T12	6	TC Tree - Crack
		T1-T6	6	TC Tree - Center
6	Corridor, Level 6	T25-T30	6	Joist Cavity
		T1-T4 (NE)	4	Stud Cavity
		T7-T12	6	TC Tree - Crack
		T1-T6, T13-T18, T19-T24	18	TC Tree - Center
TOTAL			233	



★ Thermocouples T26 to T31 arranged vertically, top down
Figure 4.3. Thermocouple layout in the southwest compartment at level 2 and adjacent space associated with Fire Test 1.

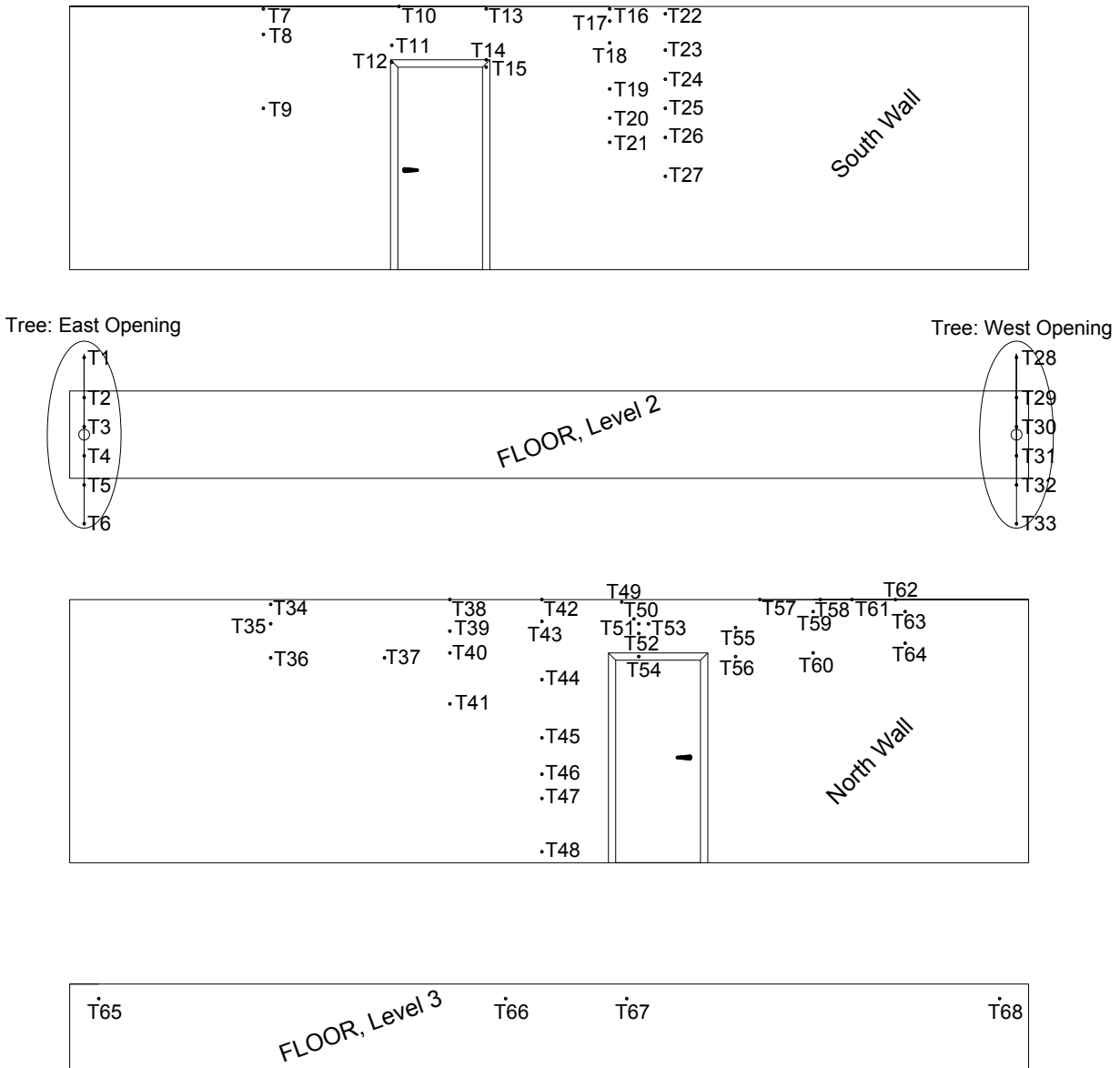


Figure 4.4. Thermocouple layout of the corridor at level 2 and adjacent space associated with Fire Test 4.

Video Cameras

Each fire compartment was equipped with a 1080p high-fidelity video camera to record the burning and physical condition of the building interior during the fire tests. The camera was positioned with a field of view on the window openings and fire rated doors. Apart from the burn room, cameras were installed in the adjacent rooms and the corridor to capture the smoke propagation and the performance of the fire rated doors during the fire tests. In addition, global view cameras were set up on the building exterior to capture the flame extensions through the

openings. Table 4.4 summarizes the video cameras location in different fire tests and also their status following the fire tests (also refer to Figure 3.4 for video cameras locations).

Table 4.4. Video camera locations and their post-test conditions.

<i>Fire Test #</i>	<i>Camera ID</i>	<i>Location</i>	<i>Post-test condition</i>
1	FT1-VC_01	South West Compartment	Destroyed
	FT2-VC_02	South East Compartment	Saved
	FT1-VC_03	Corridor	Saved
	FT1-VC_04	North East Compartment	Saved
2	FT2-VC_01	South East Compartment	Destroyed
	FT2-VC_02	Corridor	Saved
	FT2-VC_03	North East Compartment	Saved
3	FT3-VC_01	North West Compartment	Destroyed
	FT3-VC_02	Corridor	Saved
	FT3-VC_03	North East Compartment	Saved
4	FT4-VC_01	Corridor	Destroyed
	FT4-VC_02	North East Compartment	Saved
5	FT5-VC_01	Corridor	Destroyed
	FT5-VC_02	South East Compartment	Saved
	FT5-VC_03	South West Compartment	Saved
6	FT6-VC_01	South West Compartment	Destroyed
	FT6-VC_02	South East Compartment	Destroyed

Still Cameras

Periodic images were taken during all fire tests from the building exterior to study the flame characteristics and temporal fire growth (with the major focus on side flame extensions). These image data allowed for estimating the flame height and extensions for each fire test, which may be further used in the numerical validation of dynamic fire modeling.

Miscellaneous Data

Other types of data of interest, such as atmospheric temperature, pressure, relative humidity and wind velocity, were collected on each individual test day. These data were also essential for fire modeling purposes and will be summarized in a future report.

5 TEST RESULTS

This chapter presents a preliminary set of experimental results of the earthquake and fire tests. This includes the building dynamic characteristics identified using the white noise data, global building seismic response (e.g., floor accelerations, interstory drifts, residual displacements, acceleration amplification effects) during the earthquake tests, and the temperature response in the fire tests. Further investigation of the measured results and physical observations of the test building is underway. Detailed discussions of the experimental results will be available in the final reports.

5.1 System Identification Results

Low amplitude white noise tests were conducted prior to and following each earthquake test to characterize the dynamic state of the building. Using data recorded from these white noise tests, the deterministic-stochastic identification (DSI) method (van Overschee and de Moor, 1996) is used to estimate the modal parameters (natural frequencies, damping ratios, and mode shapes) of the test building. The DSI method is a time-domain system identification method that realizes a linear state-space model using input-output data. In this section, the measured floor accelerations (two each in the longitudinal and transverse directions at each floor) were used to identify the dynamic properties of the test specimen. Prior to performing the system identification algorithm, the measured accelerations (with a sampling rate of 240 Hz) are filtered using a 4th order band-pass Butterworth filter with cut-off frequencies at 0.15 Hz and 30 Hz. This frequency range includes all the vibration modes that contribute noticeably to the building response. The filtered accelerations are subsequently resampled to 80 Hz to facilitate the computational efficiency of the system identification process.

Figure 5.1 presents the identified modal periods and damping ratios of the first longitudinal (1-L) and torsional (1-To) vibration modes of the building during the 3% g RMS white noise tests. The corresponding mode shapes of the identified modes are illustrated in Figure 5.2. It is noted that the building state at various stages during the testing phase are defined earlier in Table 3.4. As shown in the figure, the initial building periods (corresponding to S0) were 0.28 second for the longitudinal mode (as compared to the code-base period of 0.43 second) and 0.24 second for the torsional mode. The building periods remained essentially constant between S0 to S5

(following the 50% design level earthquake). The longitudinal period elongated substantially to 0.54 second at S6 (following the design event) and further to 0.84 second at S7 (following the MCE event). Similarly, the building torsional period also sustained significant increase during the design and MCE events (period increased to 0.47 second at S7). The damping ratios also increased appreciably following the design event, however no further increase was observed following the MCE event. Comparison of the building states before and after the fire tests (S7 and S8) indicates that the fire tests only noticeably decreased the damping ratios rather than causing significant building period elongation. This further indicates that the initial stiffness of the earthquake-damaged building remained largely unaffected by the fire tests. It is noted, however, the white noise test results are not effective for assessing the post-fire nonlinear behavior of the building as a result of the low amplitude associated with the tests.

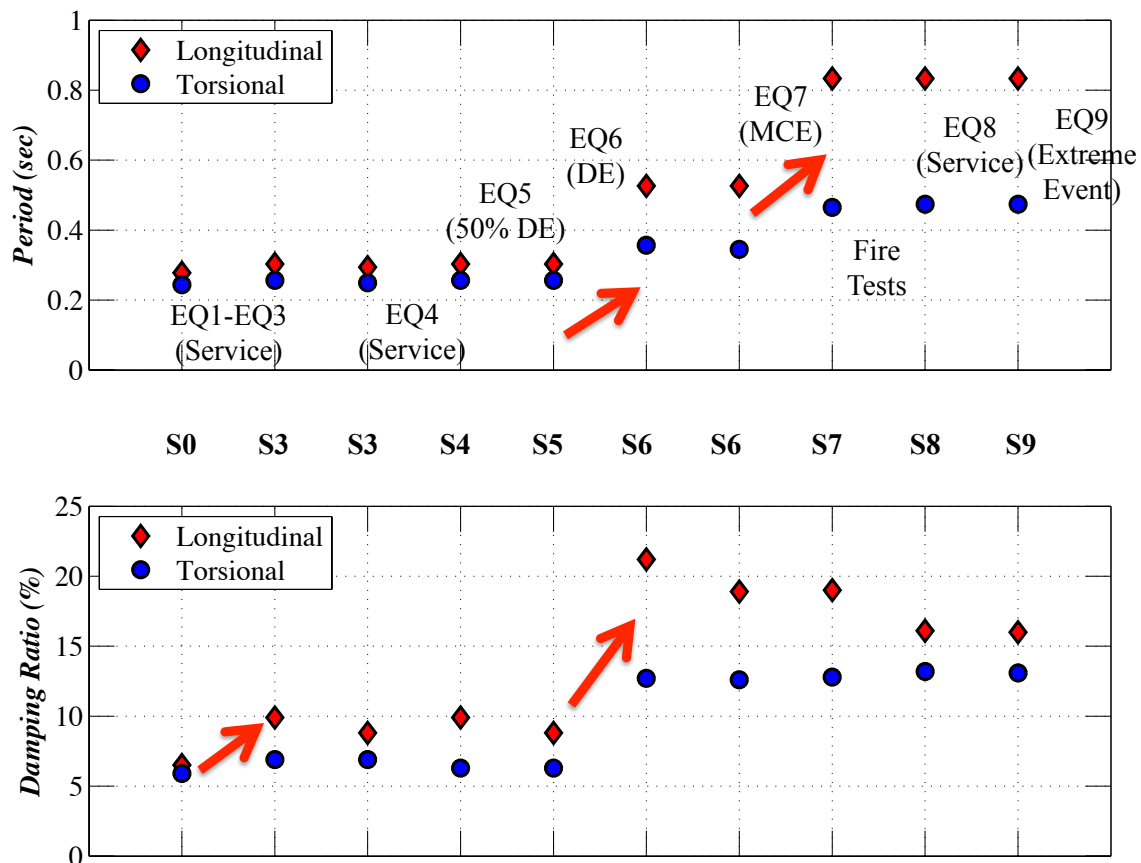


Figure 5.1. Identified modal periods and damping ratios of the first longitudinal and torsional vibration modes of the test building during 3% g RMS WN tests.

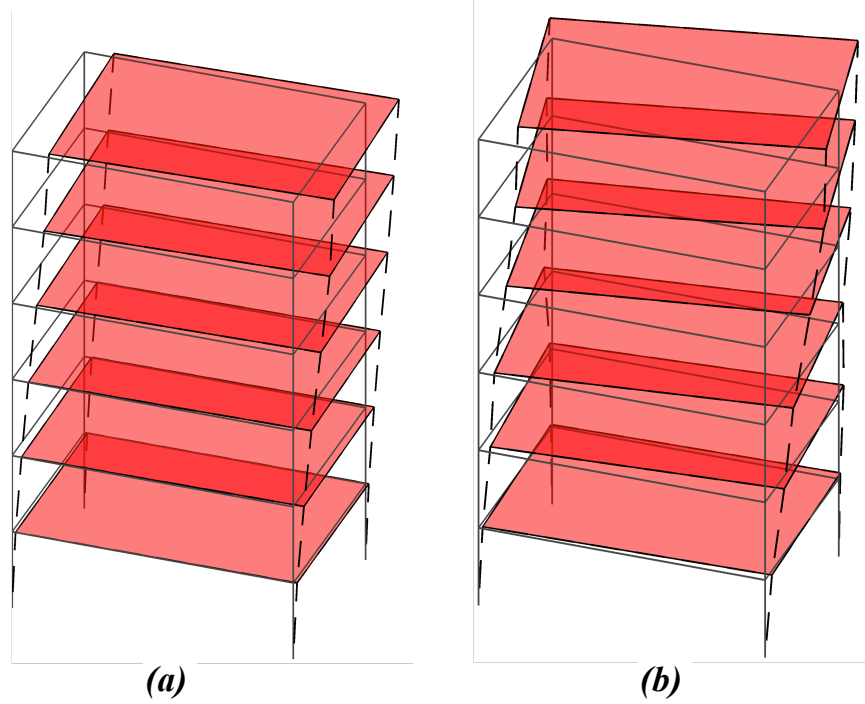


Figure 5.2. Identified mode shapes associated with the initial state (S0): (a) mode 1-L, and (b) mode 1-To.

5.2 Earthquake Test Results

Measured absolute floor accelerations obtained during the earthquake tests were obtained by averaging the accelerations measured at the four corners of each floor. Subsequently, the absolute floor displacements were obtained by double integrating the measured floor accelerations, and the displacements determined using the double integration method were verified by displacement directly measured by the string potentiometers at the lower floors and the GPS system on the roof. The interstory drift ratios of the building were subsequently calculated as the difference of two averaged displacement histories between sequential floors normalized by the floor height. While the uncertainty of the measured accelerations was relatively low (with an estimated errors of ± 0.002 g), the reported building floor displacements (and interstory drifts) were subjected to larger uncertainties since they were double integrated using the measured accelerations. The relative error of the displacement measurements were within the range of 5% and 10%, depending on the level of building nonlinearity during the earthquake tests (Skolnik and Wallace, 2010). Furthermore, the roof absolute displacements are obtained by combining the collocated GPS and accelerometer measurements using a Kalman

filter (Bock et al., 2011), which are further used for determining the transient and residual roof drift response of the building for each earthquake test.

5.2.1 Peak Building Response

Table 5.1 summarizes the peak building responses during each earthquake test, which include peak floor accelerations (PFAs), peak inter-story drift ratios (PIDRs), peak roof drift ratios (PRDRs), and residual roof drift ratios (RDR_{res}). It is noted that the building sustained very large residual drift following the test EQ9 (above 1% residual roof drift and about 6% residual inter-story drift at level 2), thus double-integrated floor displacements may be ineffective for capturing the shifted baseline. As a result, the interstory drift ratios associated with test EQ9 at the lower three levels are determined using direct displacement measurements from string potentiometers, while the roof displacement was obtained by combining the collocated GPS and accelerometer measurements as previously discussed.

Table 5.1. Peak building responses during the earthquake tests

<i>Test Motion</i>	<i>PFA (g) (Floor #)</i>	<i>PIDR (%) (Level #)</i>	<i>PRDR (%)</i>	<i>RDR_{res} (%)</i>
EQ1:RIO-25	0.35 (R)	0.08 (L4)	0.05	0.0
EQ2:CNP-25	0.38 (R)	0.09 (L4)	0.07	0.0
EQ3:CUR-25	0.45 (R)	0.10 (L4)	0.08	0.0
EQ4:CNP-25	0.43 (R)	0.10 (L4)	0.09	0.0
EQ5:CNP-50	0.85 (R)	0.24 (L3)	0.19	0.0
EQ6:CNP-100	2.07 (R)	0.89 (L4)	0.70	0.0
EQ7:CNP-150	3.77 (F5)	1.70 (L4)	1.49	0.1
EQ8:RIO-25	0.16 (R)	0.17 (L3)	0.12	0.0
EQ9:RRS-150	4.43 (F5)	12.15 (L2)	2.84	1.2

PFA – peak floor acceleration; PIDR – peak interstory drift ratio; PRDR – peak roof drift ratio; RDR_{res} – residual roof drift ratio.

Figure 5.3 presents the building PFA and PIDR responses during the service level events (tests EQ1—EQ3 and EQ8). The seismic demands on the building were relatively low during service-level scaled earthquakes, with the PIDR lower than 0.2% and PFA lower than 0.5 g. It is noted, however, that the building observed apparent acceleration attenuation effects and larger interstory drifts for post-fire test EQ8. This is due to the fact that the test building was substantially softened due to damage accumulated during the prior earthquake tests and the fire tests.

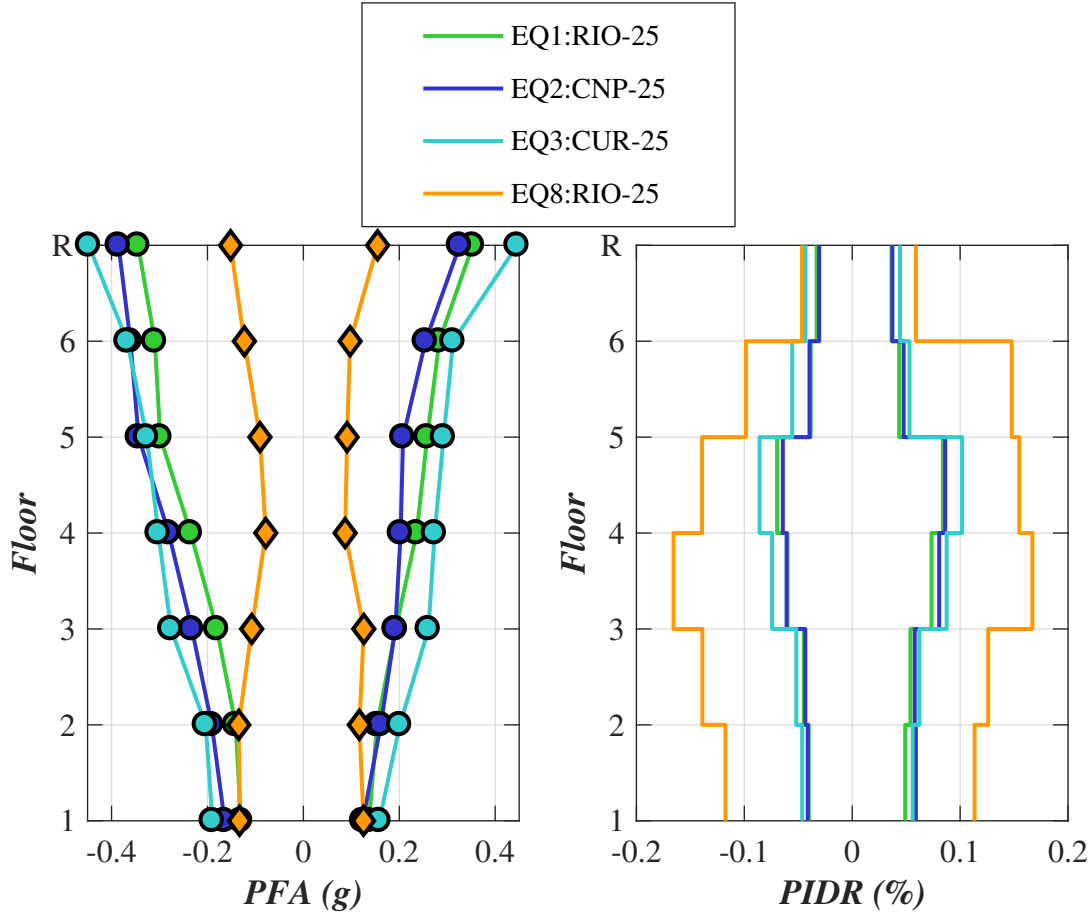


Figure 5.3. Building peak responses during the service level tests: (a) peak floor accelerations, and (b) peak interstory drift ratios.

Figure 5.4 presents the building PFA and PIDR responses during the above-the-service-level events (i.e. tests EQ5—EQ7 and EQ9). As the motion intensity increased, the largest PIDR reached about 1.0% during the design motion (test EQ6) and above 1.5% during the MCE motion (test EQ7). It is also revealed that the largest PIDR occurred at the mid-height of building (level 3 and 4) throughout the pre-fire earthquake test sequence. These results are consistent with building physical observations discussed later. In addition, the PFA increased almost monotonically up the height of the building during the pre-fire earthquake test sequence, indicating a fundamental-mode dominant structural response in these tests. The last earthquake test (near-fault MCE event EQ9) subjected the building to extremely large drift demands (an interstory drift ratio of above 12% at level 2) and resulted in a near-collapse condition of the specimen. It is also noted that the residual (permanent) RDR of building exceeded 1% following the test (Table 5.1). This is partially attributed to the fire-induced damage to the gypsum

sheathing at level 2, which reduced the shear capacity of the shear walls, helping facilitate formation of a soft-story mechanism during the final near-fault earthquake (EQ9).

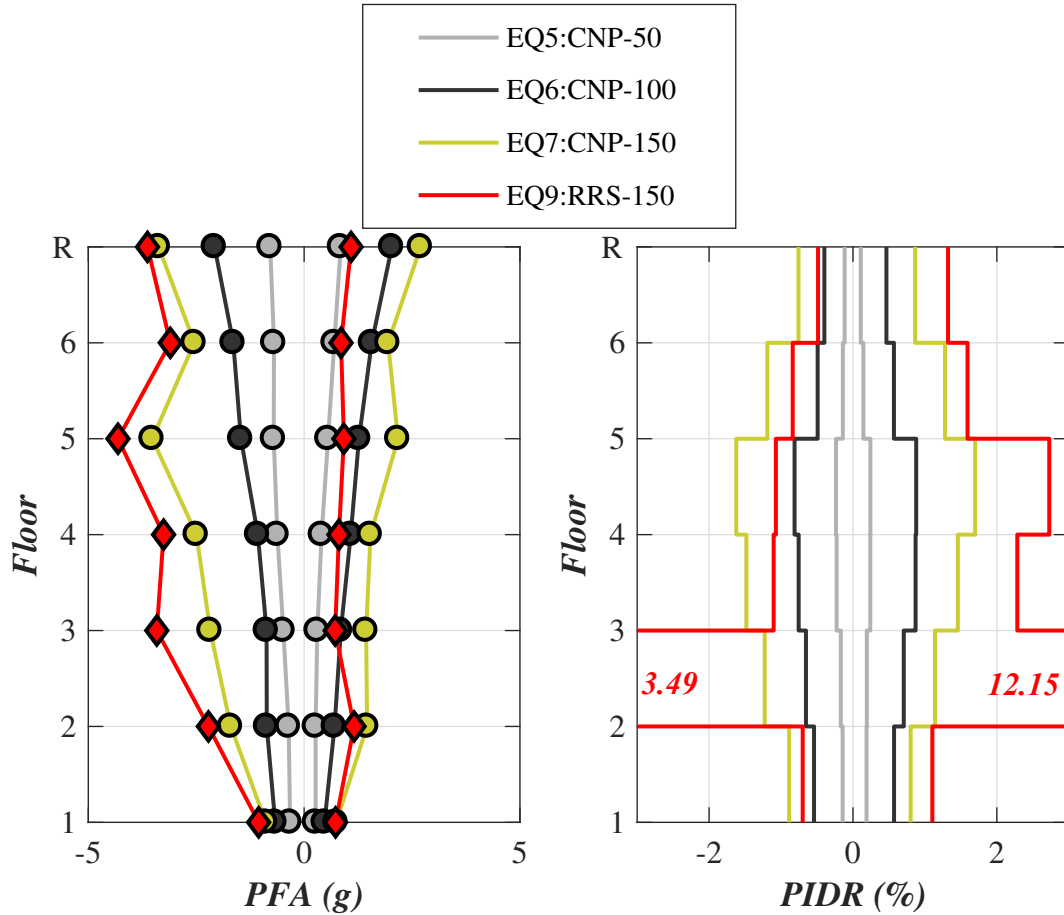


Figure 5.4. Building peak responses during above-the-service-level tests: (a) peak floor accelerations, and (b) peak interstory drift ratios.

5.2.2 Residual Displacements

As shown in Table 5.1, the test building sustained extremely large residual displacement demands during the last earthquake test (EQ9). Figure 5.5 presents the absolute displacement and interstory drift ratio time histories of the lower three levels during test EQ9. It is noted that the displacements were measured directly using the string potentiometers located on the east side of the building. As clearly shown in the figure, the residual displacements at the lower two floors were relatively small (< 1 cm) but increased significantly to 19 cm at floor 3 and 20 cm at level 4, indicating that about 90% of the residual building drift was concentrated at level 2. This observation is further demonstrated by comparing the residual interstory drift results of level 2 with the adjacent levels (about 6% at level 2 as compared to only 0.4% for level 3 and 0.2% for

level 1). The transient PIDR at level 2 were also significantly larger than those of the adjacent levels, attaining a value of about 12% in the positive (east) direction and above 4% in the negative direction.

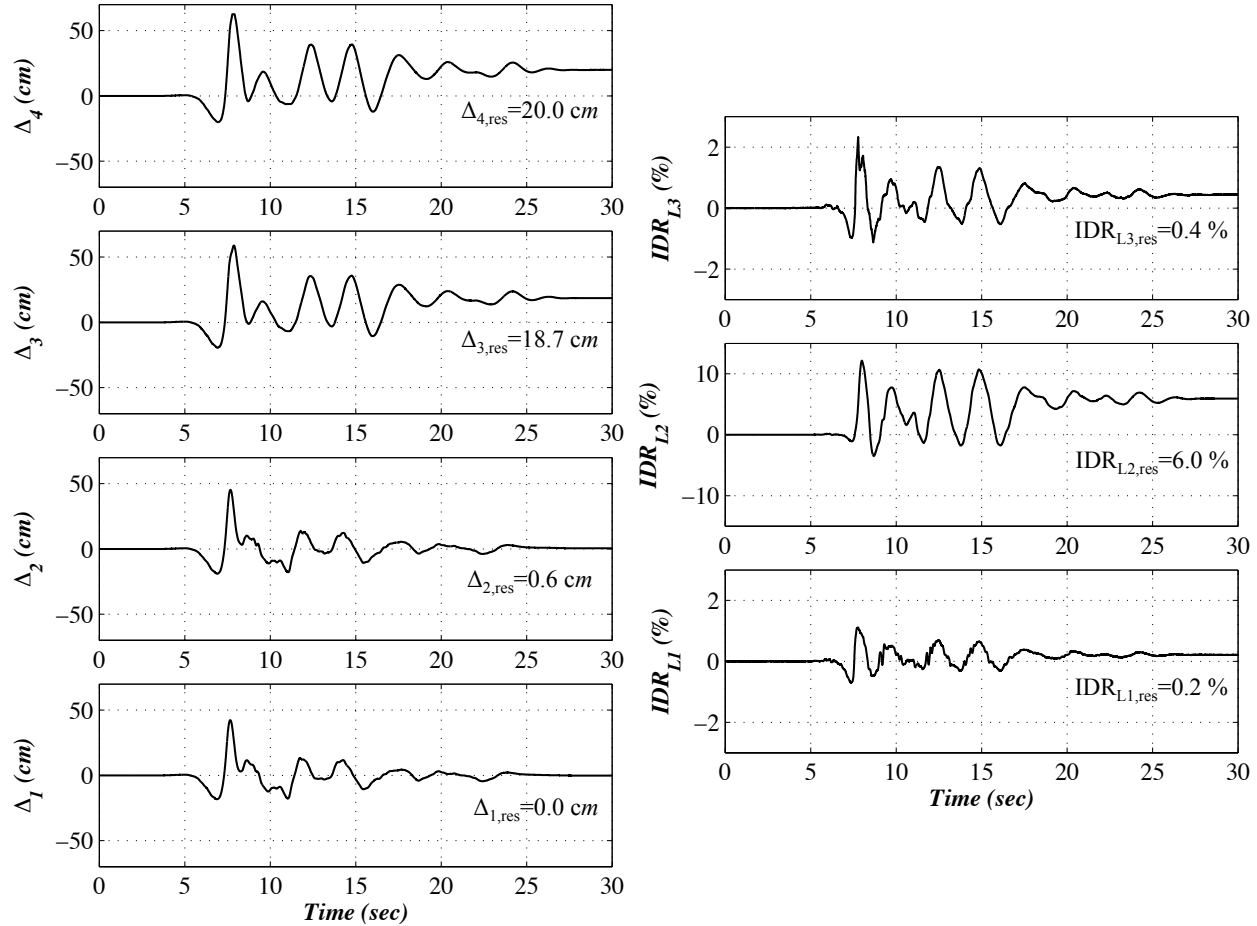


Figure 5.5. Time histories of the absolute displacement of the lower four floors and interstory drift ratio of the lower three levels during test EQ9.

5.2.3 Acceleration Amplification

Figure 5.6 presents the acceleration amplification factor Ω of the test building during the earthquake tests. The acceleration amplification factor Ω is determined as the ratio between the peak acceleration achieved at each floor and the peak acceleration of the input motion. According to ASCE 7-10 (ASCE, 2010) code provisions, the amplification factor is empirically defined as $1+2z/h$ (z/h denotes the normalized building height), which represents a linear distribution along the building height from 1.0 at the base to 3.0 at the roof. During the pre-fire service test sequence (EQ1-EQ3) (Figure 5.6a), the acceleration amplification factors increased monotonically up the height of the building with the largest values ranging between 2.0 and 2.5

at the roof, which was slightly lower than the code-specified value of 3.0. However, as the building sustained significant period elongation prior to the post-fire service level test EQ8, the attenuated acceleration distribution was observed along the building height (Ω close to 1.0). The amplification effects continued to increase during tests EQ5 and EQ6 as the motion intensity increased (Figure 5.6b). It is noted that the amplification distribution achieved during the design event (test EQ6) matched well with the code-specified distribution along the building height. During the two MCE events (tests EQ7 and EQ9), the observed floor amplification effects were significantly larger than the code-specified distribution at all floors (Figure 5.6b). This is due to the presence of impulse-like acceleration spikes during these tests.

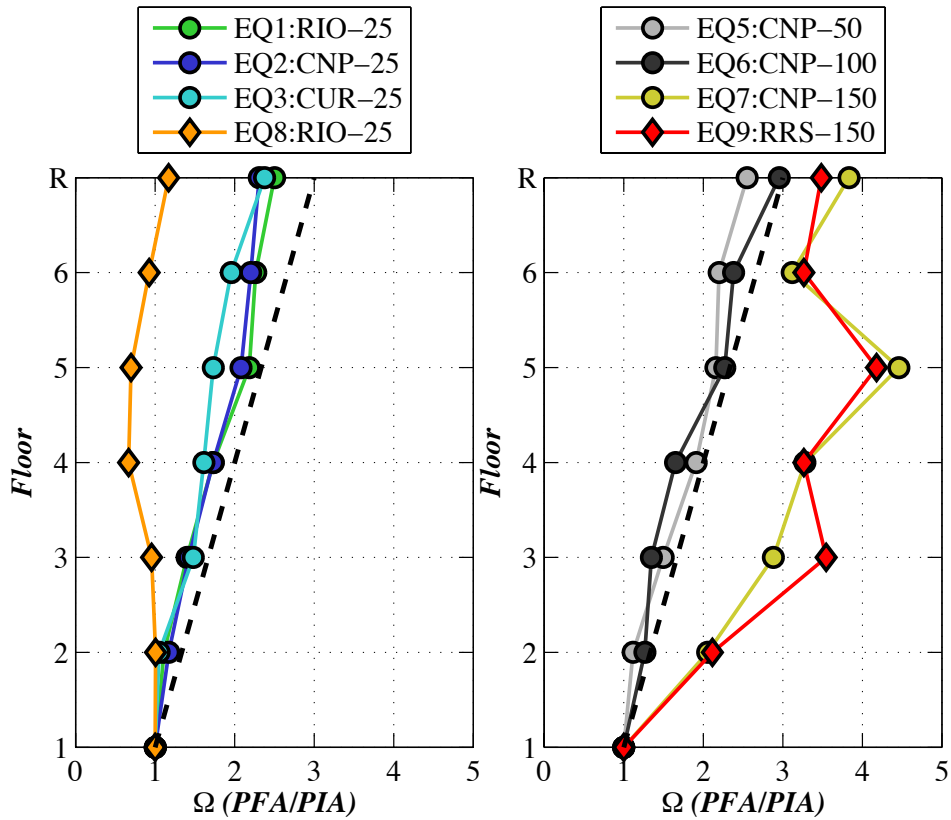


Figure 5.6. Acceleration amplification factor of the test building under: (a) service level tests, and (b) above-the-service level tests.

5.3 Fire Test Results

Table 5.2 summarizes the burn durations and maximum temperatures achieved for all fire tests. A post-flashover burn condition was achieved in each test as anticipated and calculated using existing ventilation. It is noted that the burn durations and the maximum achieved room

temperature of individual fire tests varied depending on the compartment ventilation and atmospheric conditions. As shown in the table, four out of six tests measured a compartment temperature exceeding 1000 °C, which closely agrees with the pre-test numerical simulation results. Ventilation was observed as the governing factor in the southeast compartment at level 2 (Fire Test 2), where the window opening dimensions were reduced by partially blocking it using 16 mm (5/8”) thick Type-X gypsum panels, in an attempt to regulate the ventilation condition and achieve a typical post-flashover condition.

Table 5.2. Burn duration and achieved maximum temperature.

Test #	Burn location	Burn duration, t (s)	Max. temperature T_{max} (°C)	Time @ T_{max} (s)	Location T_{max}
1	Level 2, Southwest Compartment	480	1015	143	Center TC Tree, 1.6m from ceiling
2	Level 2, Southeast Compartment	960	851	348	Center TC Tree, 1.6m from ceiling
3	Level 2, Northwest Compartment	540	1033	533	Center TC Tree, 1.6m from ceiling
4	Level 2, Corridor	850	894	332	Door Frame Cavity, North Wall 0.56 m from ceiling
5	Level 6, Corridor	720	1077	552	Door Frame Crack, South Wall, 0.08 m from ceiling
6	Level 6, Southwest Compartment	660	1049	464	Wall Crack on Internal North Wall, 0.08 m from ceiling

Figure 5.7 presents the temperature response of the burn room (the southwest compartment at level 2) during Fire Test 1. These temperatures were measured by the thermocouple tree located at the approximate center of the fire compartment. As shown in the figure, the maximum temperatures exceeded 1000 °C in less than 180 seconds, which was recorded by thermocouple SW-T31 located at 1778 mm below the ceiling (the lowest one on the thermocouple tree). This is indicative of reaching the flashover conditions in the burn compartment within one minute following the ignition. The upper layer compartment temperatures reached ~950 °C at 450

seconds from the ignition (SW-T28 at a distance of 457 mm and SW-T29 at a distance of 762 mm from the ceiling, respectively), while the compartment temperatures at the middle layer (1067 mm and 1372 mm from ceiling) were as low as 200 °C. This clearly indicates a highly non-uniform temperature profile along the vertical direction of the compartment (burn room). It is also noted that all the temperature response were characterized by a double-peak pattern (with the first peak occurring at < 180 seconds and the second one at ~450 seconds), possibly due to the atmospheric effect on the compartment fire dynamics following the flashover. Thereafter, the compartment temperatures dropped abruptly to less than 400 °C, which is indicative of the total burnout of fuel.

Figure 5.8 presents the temperature response of the stud cavity around the burn room during Fire Test 1, while Figure 5.9 presents the temperature response of the ceiling joist cavity above the burn room during the same test. It is observed the stud cavity measured high temperatures (> 900 °C) at three locations (SW-T11, SW-12 and SW-T19), while the temperatures measured at the remaining two locations (SW-T13 and SW-T15) were significantly lower (< 150 °C). The high temperatures may be due to the fact that the thermocouples were located on a metal surface inside of the CFS framing. In addition, the drastic temperature increase of SW-T19 (from ambient temperature to ~450 °C) between 60 and 70 seconds implies the loss of thermal barrier for the CFS wall (dehydrated or crumbled gypsum with surface cracks), thus significantly increasing the heat transfer rate through the wall thickness. In contrast, the joist cavity temperature remained relatively low (with the highest maximum temperatures of about 100 °C). This is likely due to the fact that the gypsum board ceiling provided an effective thermal barrier.

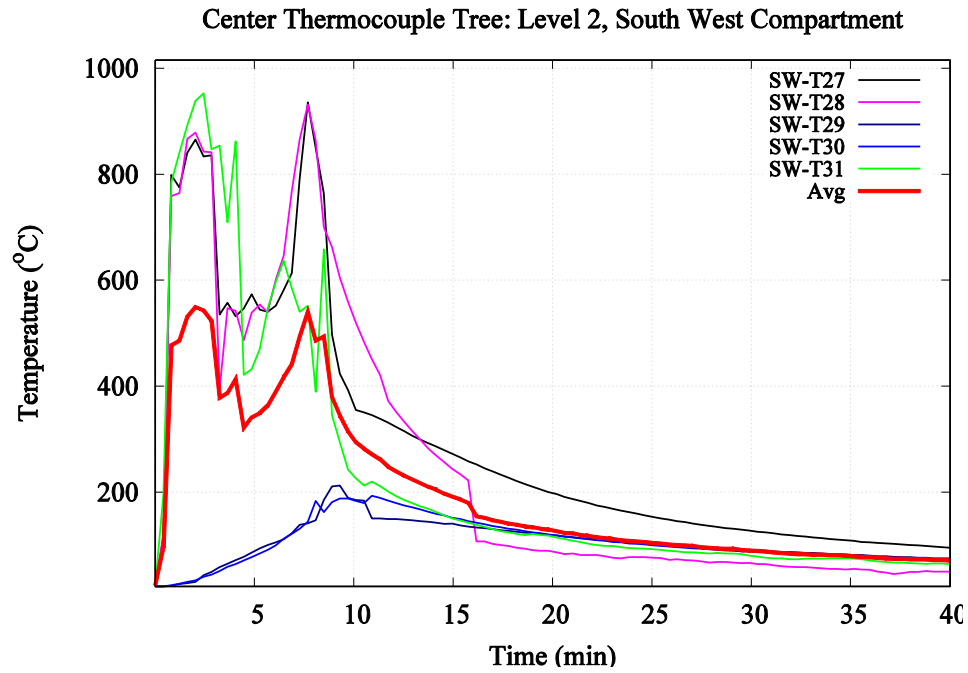


Figure 5.7. Temperature response of the southwest compartment at level 2 (burn room) – Fire Test 1.

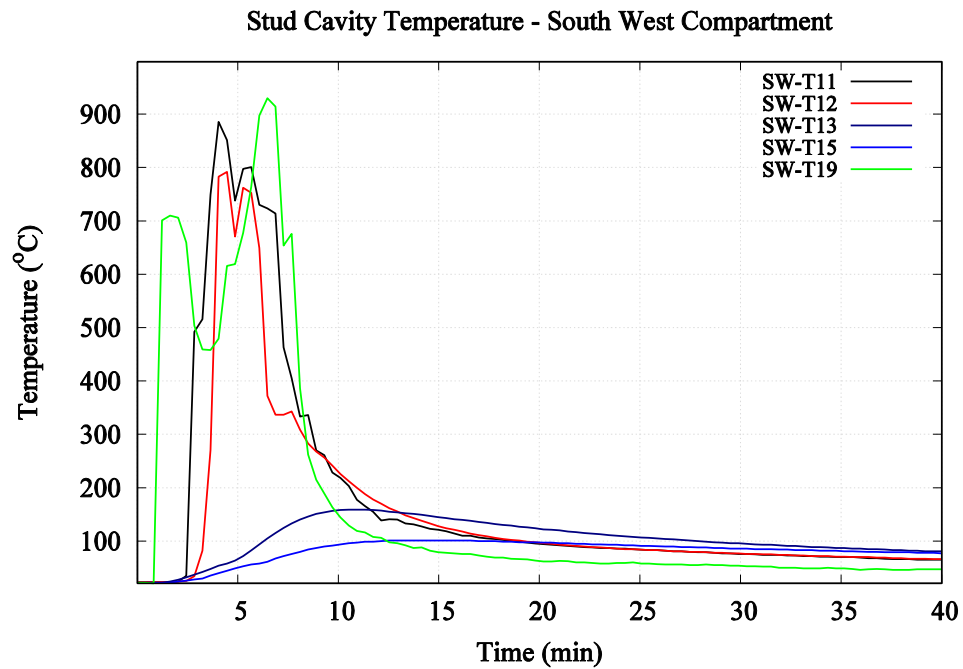


Figure 5.8. Temperature response of the stud cavities in the southwest compartment at level 2 – Fire Test 1.

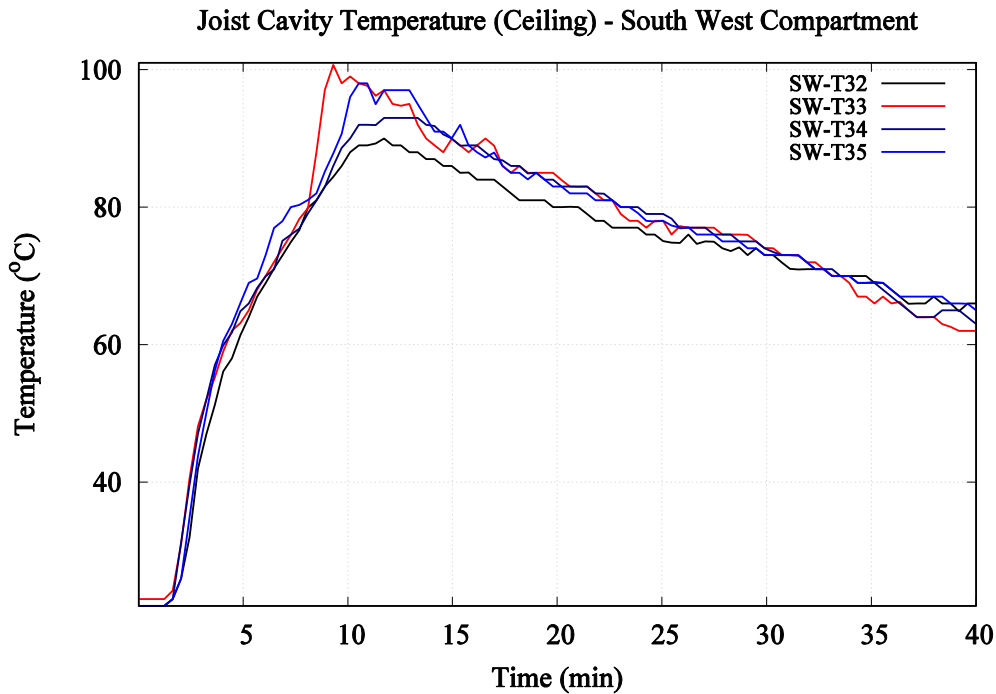


Figure 5.9. Temperature response of the ceiling joist cavities above the southwest compartment at level 2 – Fire Test 1.

Figures 5.10 and 5.11 present the temperature response of the east and west ends of the level 2 corridor during Fire Test 4, respectively. Due to the presence of eastward wind during the fire test (with a speed between 5km/h to 13 km/h), the opening at the west end of the corridor was about 0.6 m high from the floor, while the one the east end was about 1.2 m from the floor. The wind effect also resulted in higher temperatures at the east end of the corridor. As shown in Figure 5.10, the measured maximum temperature at the east end of the corridor ranged from 650 °C (for the thermocouple close to the ceiling) to about 900 °C (for the lowest thermocouple at 1.8 m below the ceiling), while the maximum temperatures at the east end reached only less than 600 °C (Figure 5.11). In addition, it is noted that higher temperatures were observed in the upper layer at the west end of the corridor, while the upper layer temperature at east end of the corridor was appreciably lower compared with the temperature of the lower layer.

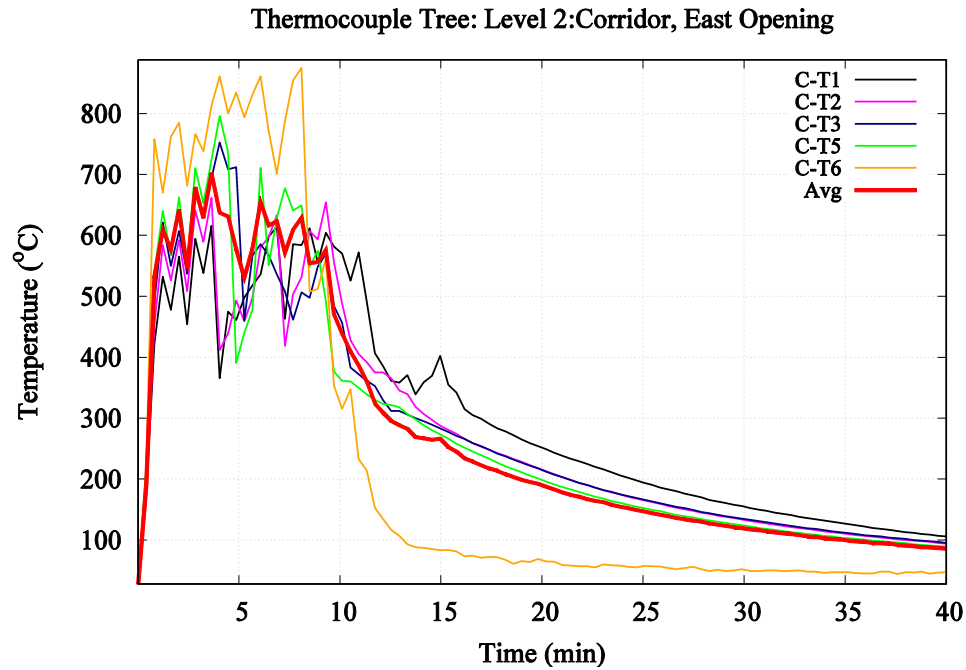


Figure 5.10. Temperature response of the east end of the corridor at level 2 – Fire Test 4.

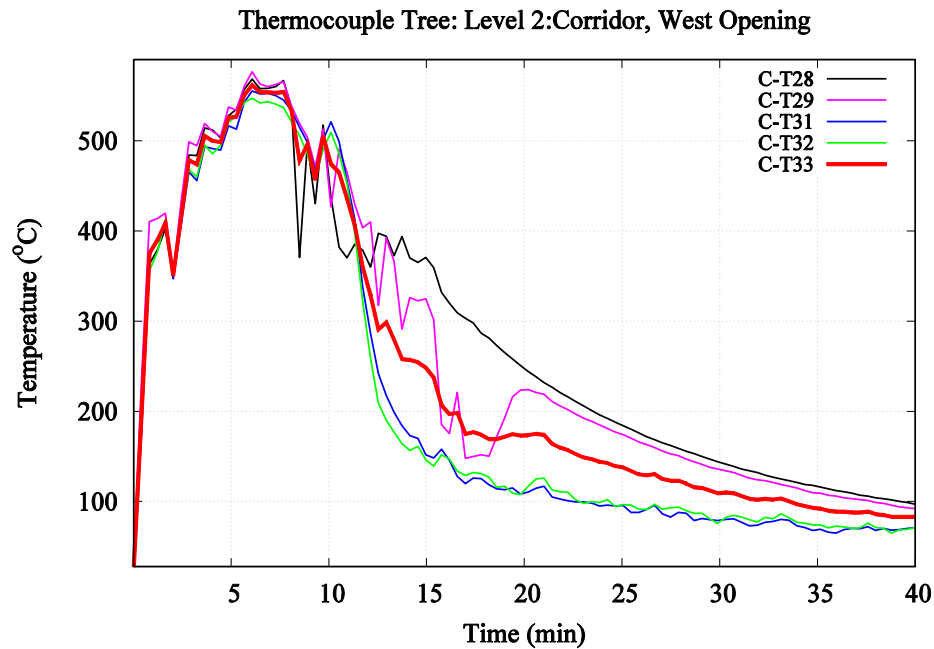


Figure 5.11. Temperature response of the west end of the corridor at level 2 – Fire Test 4.

Figure 5.12 shows the flame and smoke extension from the compartment openings during Fire Tests 1 and 4. During Fire Test 1 (southwest compartment of level 2), flames and smoke were fully developed 45 seconds following the ignition and spread out from the window opening (Figure 5.12a). As observed from visual observations and recorded video footage, the flame

height extended ~ 3 m vertically and ~ 1 m horizontally. In addition, smoke also spread out from the window opening of the adjacent compartment, indicating the propagation of smoke through the adjacent compartment due to the failure of the fire-rated door. During Fire test 4 (the corridor at level 2), flame and smoke was observed at the opening at the east end of the corridor in about 40 seconds from ignition. While the flame extension was contained by eastward wind in the initial burning stage, the flame extended up by 3.0 m and the smoke up to 6.0 m in about 150 seconds from ignition due to the prevailing wind condition. In addition, the horizontal flame extended 1.8 m due to the congruent nature of the direction of wind flow and the openings that created a ‘tunnel effect’. This is confirmed by the absence of flame extension around the opening at other end of the corridor. Smoke propagation from the corridor to the adjacent compartments was also observed in this test. This revealed the ineffectiveness of fire-rated door and gypsum wallboard in containing the flame and smoke spread.



Figure 5.12. Flame and smoke extension from the compartment openings: (a) Fire Test 1, and (b) Fire Test 4.

5.4 Physical Observation

5.4.1 Structural System

As presented in Table 3.4, detailed inspection of the test building was conducted at six stages throughout the test program to characterize the physical damage of the building structure and the nonstructural components. The detailed inspection stages included: pre-EQ1 (associated with state S0), post-EQ3 (associated with state S3), post-EQ6 (associated with state S6), post-EQ7 (associated with state S7), post-fire (associated with state S8), and post-EQ9 (associated with state S10). On the test dates with multiple earthquake tests, rapid inspection was also conducted in the middle of the test sequence. Damage documentation relied upon visual inspections as well as detailed photographs. It is noted that the first three inspections focused only on the damage to the wall sheathing, since the wall framing was enclosed. During the post-EQ7 inspection, the corridor shear wall gypsum panels at select location of level 4 were removed to identify the seismic damage to the wall interior. Detailed inspection of the interior conditions of all shear walls and gravity walls was conducted during the post-EQ9 inspection.

As the seismic demand of the building was relatively low during the pre-fire service level tests ($PIDR < 0.2\%$), the sheathing panels sustained only limited damage in the form of incipient screw withdrawal and the bulged (or crushed) sheathing panel at the corner or edge (Figure 5.13a-b). Damage continued to develop during tests EQ5 and EQ6 (design event) as the seismic drift demand increased. The post-EQ6 inspection revealed that the screw withdrawal became extensive on the longitudinal shear and gravity walls at level 3 and 4 as the PIDR at these two levels reached about 1.0%. In addition, buckling of the sheet steel (below the rim tracks) of the corridor wall composite panels at level 1 (Figure 5.13c) was detected in the post-EQ6 inspection stage, although this damage mechanism was caused by the large gap height due to the discontinued sheathing gypsum. As the PIDR reached above 1.5% during the MCE event (test EQ7), the corridor walls underwent apparent crushing at the boundaries between the shear walls and the gravity walls (Figure 5.13d) at level 3 and 4. This resulted in partial detachment of the gravity wall gypsum panels around the doorframes and out-of-plane distortion of the shear wall composite panels. Buckled sheet steel of the corridor shear wall sheathing was detected during the wall interior inspection of the level 4 shear walls (Figure 5.13e), however the corner walls and all the shear wall framing sustained no apparent damage despite of the large drift demands

(PIDR > 1.5%). In addition, rim track flange buckling was detected at several locations of at level 3 and 4 (Figure 5.13f).

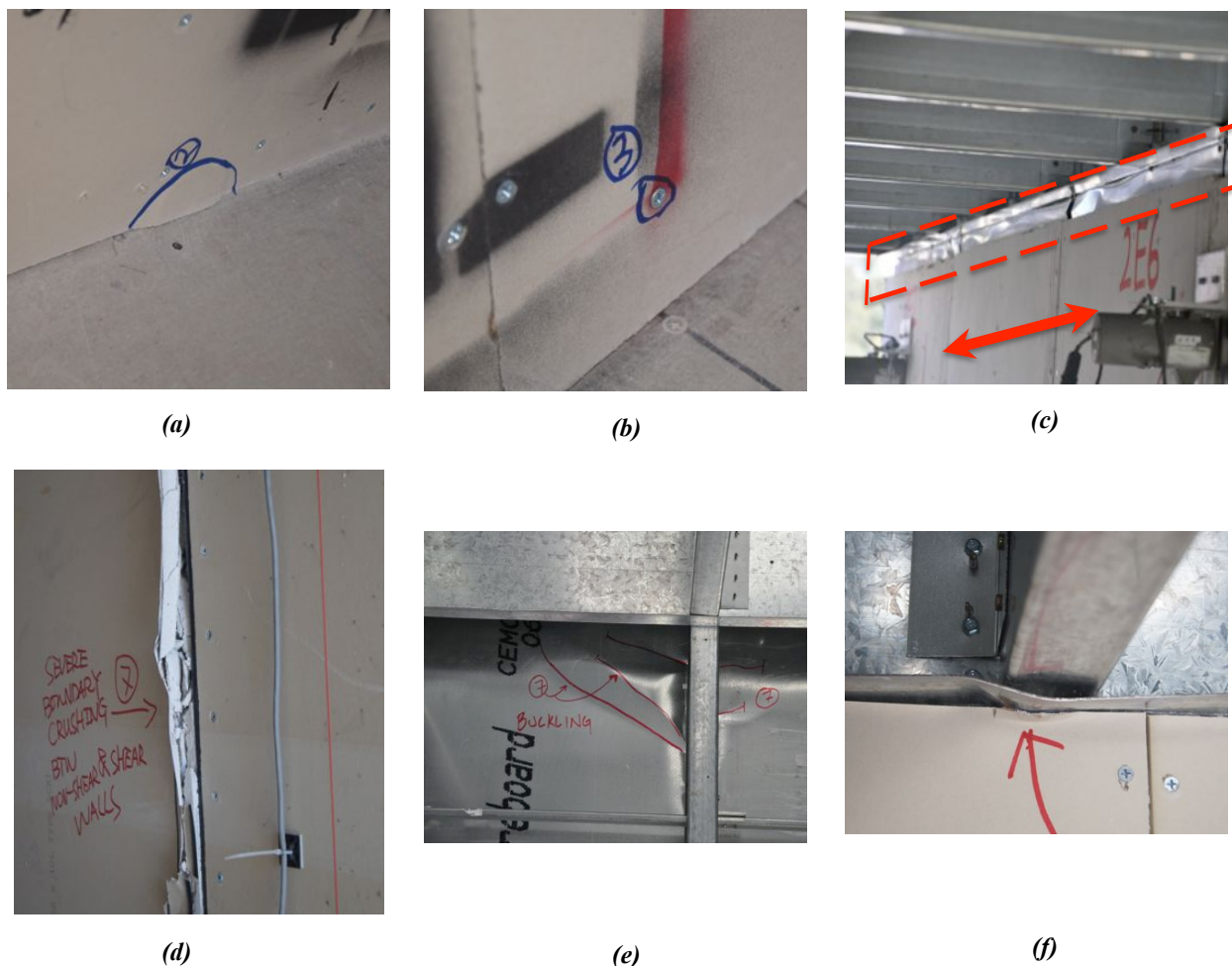


Figure 5.13. Damage to the test building during the pre-fire earthquake test sequence: (a) gypsum bulging on the bottom edge (EQ2), (b) gypsum screw popping (EQ3), (c) buckled sheet steel of corridor shear wall at level 1 (EQ6), (d) sheathing panel crushing between the shear wall and gravity wall at level 4 corridor (EQ7), (e) buckled composite panel sheet steel of corridor shear wall at level 4(EQ7), and (f) buckled rim track flange above gravity wall at level 4 (EQ7).

Following the MCE earthquake event, live fire tests were conducted at six burn rooms at level 2 and 6. The elevated temperatures caused complete calcination of the wall and ceiling sheathing (gypsum wallboards and fiber-reinforced cement floorboards) and charred or melted doors (Figure 5.14a-b). The sheathing damage resulted in significant strength and rigidity loss of the structural components. Observed damage to the building structural system occurred in the form of: (1) partial detachment of gypsum ceilings (Figure 5.14c), and (2) significant deflections

(about 1.5 cm) of the floor system at the second floor as a result of deteriorated cement boards on top of the sheet steel (Figure 5.14d).

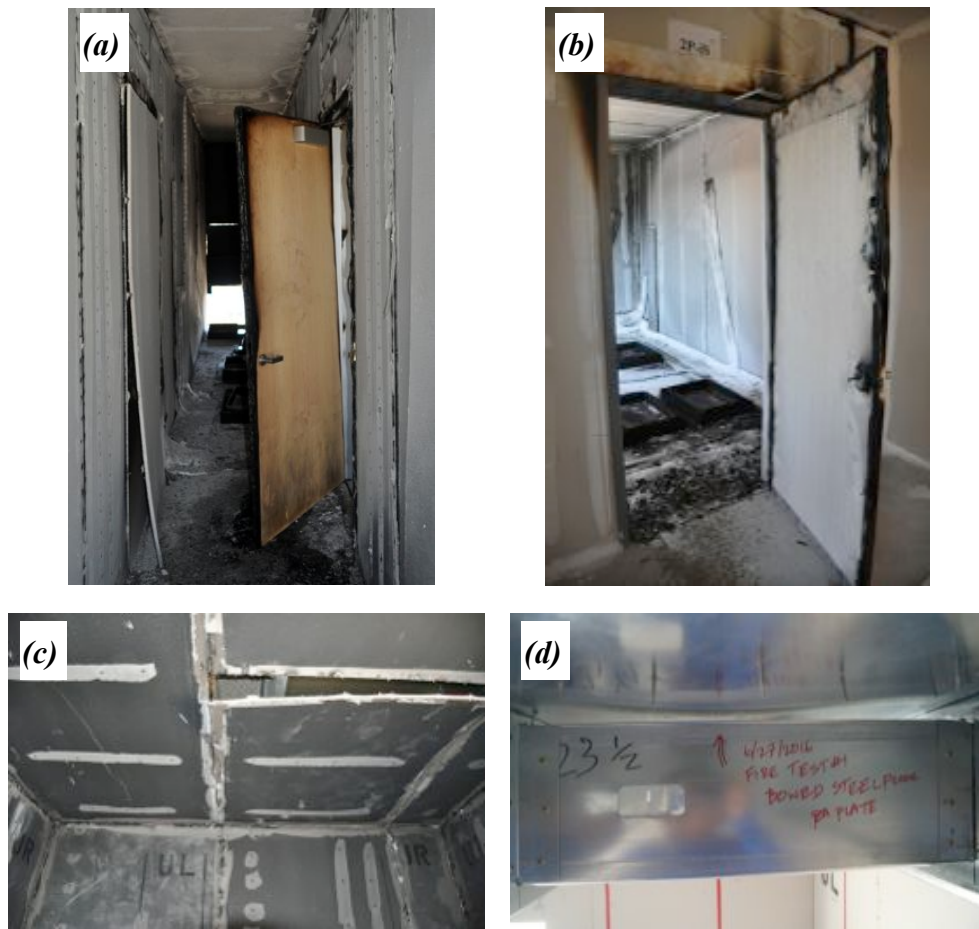


Figure 5.14. Damage to the test building following the fire tests: (a) level 2 corridor, (b) partially detached door, (c) partially detached gypsum ceiling, and (d) sagging floor system at the second floor.

In the post-fire earthquake test sequence (tests EQ8 and EQ9), the service level aftershock test (EQ8) did not incur further damage to the building due to its low seismic demands ($PIDR < 0.2\%$ and $PFA < 0.2\text{ g}$). During the near-fault extreme earthquake event (test EQ9), the building was subjected to extremely large seismic drift demands at level 2 ($PIDR > 12\%$ and IDR_{res} of about 6%). As shown in Figures Figure 5.15c and Figure 5.16, the soft story mechanism occurred at level 2 of the building, as it is visually apparent that the building leaned eastward at the end of the test. As a result, the test building imposed extremely severe damage to its structural system. At level 2 in particular, all the corridor shear walls lost their strength due to complete panel detachment as well as the twisted and displaced framing studs (Figure 5.15a). In

addition, one instance of tension rod connection failure was observed at the longitudinal wall of the southeast corner (Figure 5.15b). The test building, however, resisted collapse largely due to redistribution of loads and framing action of the building rod tie-down system.

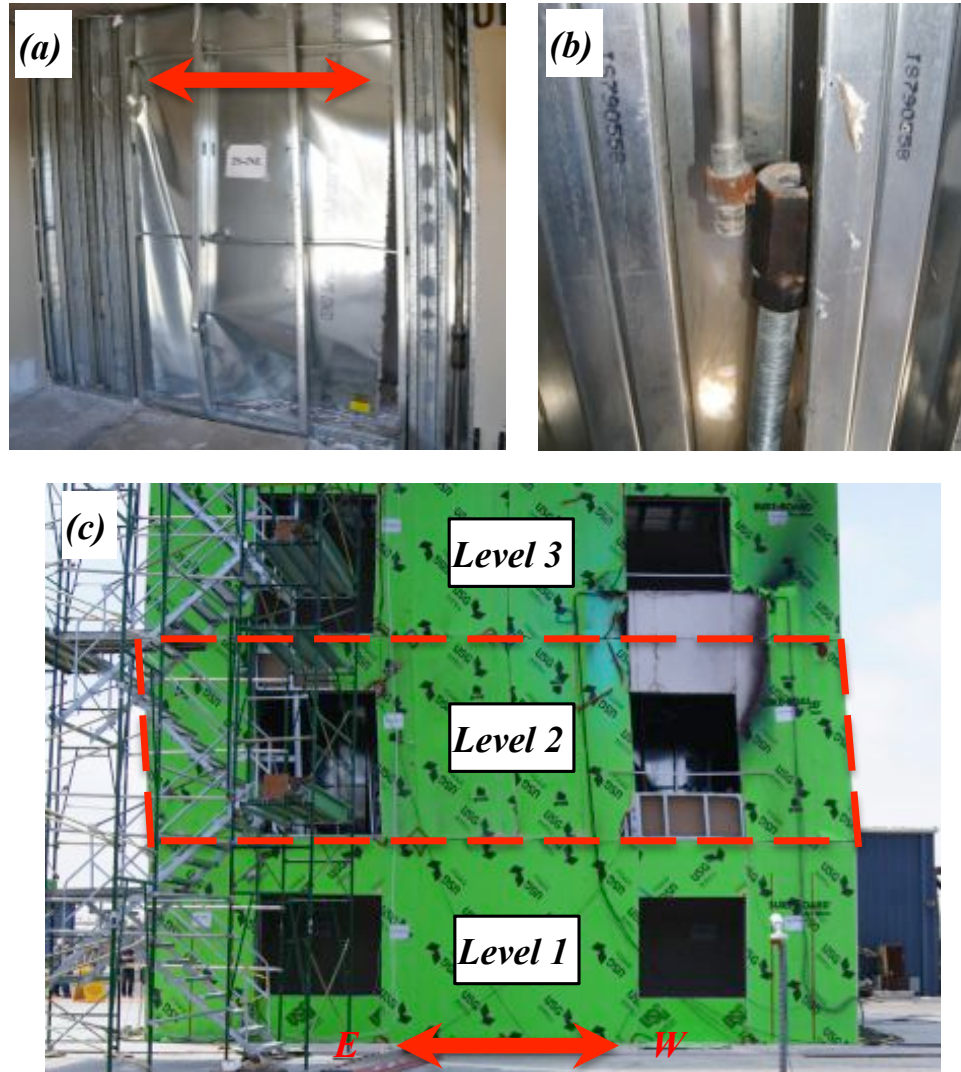


Figure 5.15. Damage of the test building at the completion of the test program: (a) severely damaged corridor shear wall at level 2, (b) dislodged tension rods at the corner shear wall at level 2 (southeast room), and (c) north façade of the building at the lower three levels with apparently residual drifts at level 2.

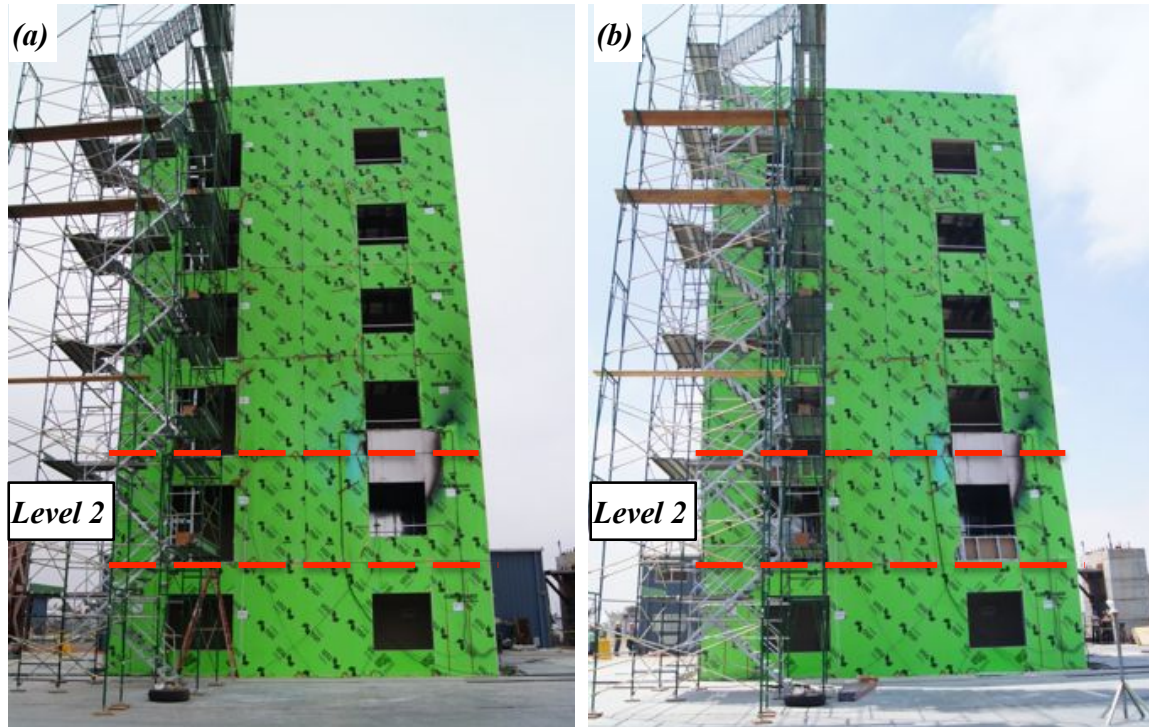


Figure 5.16. North elevation of the test building: (a) pre-EQ9 condition, and (b) pre-EQ9 condition.

5.4.2 Nonstructural Systems

Interior Partition Walls

Since all partition walls were subjected to out-of-plane seismic load during the earthquake tests, damage to the interior partition walls was minor during the pre-fire earthquake test sequence. Typical seismic damage included crushed gypsum corners and joint tape cracks at the intersection with the longitudinal structural walls. During the fire test, the partition gypsum panels completely dehydrated due to elevated temperature in the fire test compartment, although they remained attached to the steel framing.

Doors

Physical damage to the doors was inspected at four inspection stages throughout the test program: post-EQ3, post-EQ6, post-EQ7 and post-EQ9. Dependent on the severity of damage and their implications related to functionality, the observed damage was categorized into three damage states (DSs). The damage states and the associated physical damage characteristics are presented in Table 5.3, and the typical damage modes as observed during the earthquake tests are illustrated in Figure 5.17.

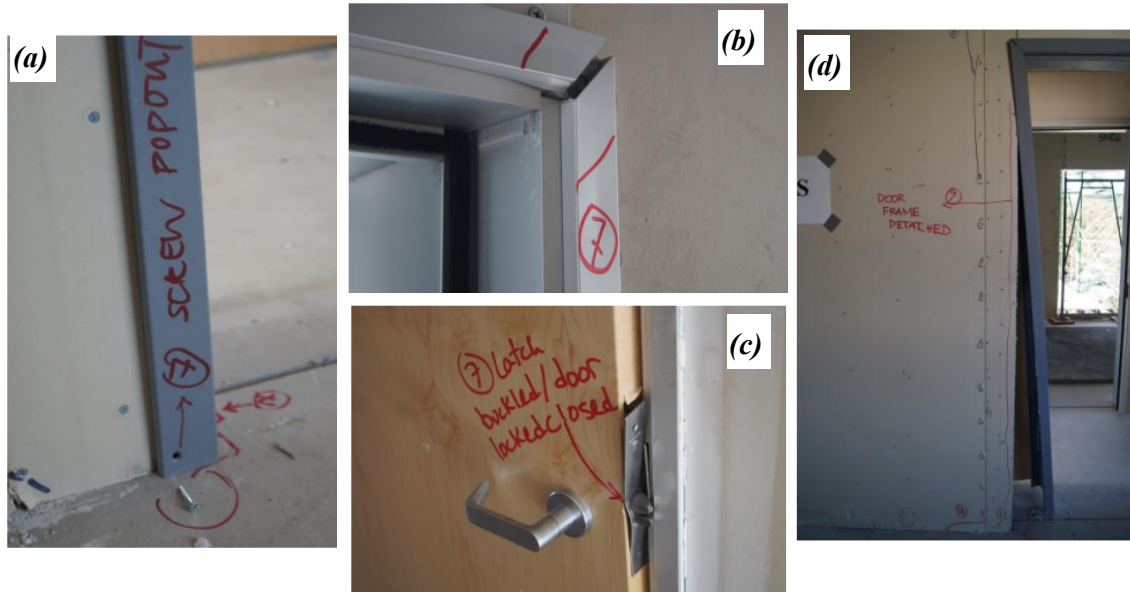


Figure 5.17. Examples of door damage: (a) door frame screw popping (DS-1), (b) door frame gapping (DS-2), (c) buckled door latch (DS-2), and (d) detached door frame (DS-3).

Table 5.3. Door damage states and the associated damage modes

<i>Damage state</i>	<i>Physical damage</i>
DS-1 (minor)	Door frame gapping, door frame screw withdrawal, door frame loosening
DS-2 (moderate)	Door jam, door frame distortion, door latch failure
DS-3 (severe)	Door frame severe distortion, door frame detachment

Table 5.4 provides a detailed summary of the door damage state and the associated damage modes at the four inspection stages during the test sequence. It is noted that the doors located in the fire compartments (all four doors at level 2 and three doors at level 6) lost their functionality following the fire testing. The observed damage occurred exclusively on the corridor doors as the corridor walls were subjected to in-plane shear distortion throughout the earthquake tests, while the doors on the partition walls sustained minimum damage. As the drift demands remained very low ($PIDR < 0.1\%$) during the service level tests (EQ1-EQ3), the doors all performed well with no visible damage. Damage initiated on four corridor doors during the design level motion ($PIDR$ reached $\sim 1.0\%$), however the observed damage remained essential minor (DS-1) (e.g., door frame screw popping (Figure 5.17a), and corner gapping (Figure 5.17b)). Damage continued to progress and became extensive during the MCE level motion EQ7 ($PIDR > 1.5\%$). All the corridor doors except one at level 1 suffered damage. The observed damage occurred in the form of detached or buckled door latch plate (Figure 5.17c), severe frame distortion, and severely distorted or detached doorframe (Figure 5.17d).

Table 5.4. Physical observations of door damage

Floor	Short name	Inspection stage							
		Post-EQ3		Post-EQ6		Post-EQ7		Post-EQ9	
		DS	Description	DS	Description	DS	Damage mode	DS	Description
1	1-NC	DS-0		DS-0		DS-1	door frame corner gapping	DS-1	frame corner gapping
	1-SC	DS-0		DS-0		DS-0		DS-0	
2	2-NR	DS-0		DS-0		DS-0		loss of functionality due to fire damage ¹	
	2-NC	DS-0		DS-0		DS-2	latch buckled unable to lock		
	2-SC	DS-0		DS-1	door frame distortion - unable to lock	DS-2	door jam		
	2-SR	DS-0		DS-0		DS-0			
	3-NR	DS-0		DS-0		DS-0		DS-0	
3	3-NC	DS-0		DS-0		DS-2	door latch plate failure	DS-2	door jam
	3-SC	DS-0		DS-0		DS-2	door jam	DS-2	door jam
	3-SR	DS-0		DS-0		DS-0		DS-0	
	2-NR	DS-0		DS-0		DS-0		DS-0	
4	2-NC	DS-0		DS-1	bent door frame, unable to lock	DS-2	door latch failure, loose door frame	DS-2	door latch failure, loose door frame
	2-SC	DS-0		DS-1	door frame screw popping	DS-2	door frame gapping	DS-3	door frame detached
	2-SR	DS-0		DS-0		DS-0		DS-0	
	2-NR	DS-0		DS-0		DS-0		DS-0	
5	2-NC	DS-0		DS-0		DS-2	door jam	DS-3	door jam
	2-SC	DS-0		DS-1	door frame distortion - unable to lock	DS-1	door frame screw popping	DS-3	door frame detached
	2-SR	DS-0		DS-0		DS-0		DS-0	
	2-NR	DS-0		DS-0		DS-0		DS-0	
6	2-NC	DS-0		DS-0		DS-1	door frame gapping	loss of functionality due to fire damage ¹	
	2-SC	DS-0		DS-1	door frame distortion unable to lock	DS-3	severe door frame distortion		
	2-SR	DS-0		DS-0		DS-0			
	2-NR	DS-0		DS-0		DS-0		DS-0	

¹ doors damaged during the fire tests were removed prior to the subsequent earthquake tests.

Appliances

The seismic performance of the appliances during the earthquake tests is presented in this section. It is noted that all the appliances were removed from the building or properly stowed in the building prior to the fire tests, and therefore the discussion only focuses on their seismic performance in the pre-fire earthquake test sequence. Physical inspections of the appliances were conducted at four different stages: post-EQ3 (following the service level motions), post-EQ5 (following the 50% design level motion), post-EQ6 (following the design level motion), and post-EQ7 (following the maximum considered earthquake motion). It is noted, however, that the post-EQ5 inspection of the appliances at level 6 was not performed due to unavailability of access. Since the two wall-mounted television sets at level 1 suffered no damage to the appliance or mount during all the earthquake tests, the remaining section focuses on the seismic performance of the gas units, water heaters, and seismic gas shutoff valves during the pre-fire earthquake tests.

Table 5.5 summarizes the performance of all the range units during the pre-fire earthquake test sequence. Regardless of the presence of restraints, none of the units observed any movement up to and including the 50% design level motion (however the drawer of a gas range unit at level 6 opened). During the design level motion (with a peak floor acceleration of ~ 0.7 g at the first floor and ~ 2.0 g at the sixth floor), one restrained unit at level 6 moved slightly due to restraint failure, while all the remaining three restrained units sustained no restraint failure and remained in position. In contrast, all the unrestrained units underwent substantive movement in the form of combined sliding and rotation (the observed displacement offsets reached as much as 8 cm for the units at level 1 and 50 cm for the units at level 6). During the maximum considered earthquake motions, the measured peak floor accelerations were >1.0 g at the first floor and ~ 3.0 g at the sixth floor. While no failure to the restraints occurred for the units at level 1, both restrained units at level 6 detached from their restraints and displaced. The unrestrained units at level 1 and level 6 observed significant movement (the displacement reached as much as 0.7 m for a unit at level 6). Although not observed during the tests, excessive sliding of a gas (or electric range) poses the potential risk of breaking the gas pipes and connections (or electrical cords and connectors) as a result of pulling.

Table 5.5. Physical observations of the range units during the pre-fire earthquake tests.

Level	Appliance unit	Physical observations			
		Post-EQ3	Post-EQ5	Post-EQ6	Post-EQ7
1	Unrestrained gas range	No movement	No movement	slid ~5 cm, slight rotation (CCW)	slid ~0.6 cm, slight rotation (CCW)"
	Restrained gas range	No movement	No movement	No movement	No movement
	Restrained electric range	No movement	No movement	Restraint held; drawer opened	Restraint held; drawer opened
	Unrestrained electric range	Rotated (~2 cm)	No movement	slid ~8 cm, rotated (CCW)	slid 23 cm, rotated (CCW)
6	Restrained gas range	No movement	n/a	restraint failed, rotated (CCW)	Broke free from restraint and anti-tip over bracket, rotated (CW); top grate bounced off
	Unrestrained gas range	No movement, drawer opened	n/a	Slid 46 cm (8 cm to side)	Slid ~28 cm (~8 cm to side)
	Unrestrained electric range	No movement	n/a	Slid 51 cm, rotated (CCW)	Slid ~71 cm, slight rotation (CCW); tether caught
	Restrained electric range	No movement	n/a	Restraint held; door and drawer opened	Broke free from restraint and anti-tip over bracket, rotated (CCW)

Table 5.6 summarizes the performance of all the water heaters during the pre-fire earthquake test sequence. As discussed previously, the four braced water heaters each utilized a different bracing strategy to attach the unit to the adjacent wall framing (e.g., plumbers tape, off-the-shelf strap, and combined conduit and plumbers tape). During the service level motions, the water heaters observed no or only slight movement (< 2 cm) due to the relatively low floor acceleration demands (< 0.15 g at floor 1 and < 0.5 g at floor 6). As the floor acceleration demands increased significantly during the design event and maximum considered earthquake motions, the water heaters performed poorly as a result of the larger slenderness ratio and concentrated mass compared to the range units. The observed undesired effects included excessive movement (translation and rotation), bracing strap and fastener failure, and two instances of tipping over (the unbraced water heater at level 1 and the one at level 6 using off-the-shelf straps) with the ensuing water or gas leakage from the broken or disconnected pipes. The drywall screw disengaged and broke the plumber's strap. The tipped-over water heater level 6 even punched into the adjacent gypsum boards and caused a ~0.5 m wide opening on the interior wall. From a fire safety perspective, damage of this kind may be considered as the loss of thermal barrier by

directly exposing the CFS framing to fire hazards. In an event of post-earthquake fire, this may increase the risk of flame impingement and severely jeopardize the structural integrity of the light-gauge framing. From a structural perspective, this undesired performance (in spite of good-quality wall installation) necessitates further research to identify robust seismic bracing details for nonstructural components.

Table 5.6. Physical observations of the water heaters during the pre-fire earthquake tests.

Level	Restraint condition	Physical observations			
		Post-EQ3	Post-EQ5	Post-EQ6	Post-EQ7
1	Unbraced	Rotated (<1 cm)	n/a	Tipped over*	n/a
	Single-wrap	No movement	n/a	Rotated, restraint held	Moved and rotated, restraint held
	Double-wrap	No movement	n/a	Moved (<1 cm), one strap fastener pullout	Moved and rotated, one strap broke
6	Unbraced	Moved towards mass plate	n/a	Tipper over (landed on mass plate)**	Moved and rotated, strap fastener pullout
	Off-the-shelf Strap	No movement	n/a	Tipped over*, strap broke	n/a
	Conduit and Plumbers tape	Moved (~1 cm northward)	n/a	Rotated	Broke free from restraint, remained standing

* the equipment was removed from the building following the inspection; ** the equipment was retrofitted using off-the-shelf bracing strap.

Table 5.7 summarizes the seismic performance of the seismic gas shutoff valves (SGSV) during the pre-fire earthquake test sequence (the SGSV makes and models also specified in the table). It is noted that these off-the-shelf motion-activated SGSVs were mounted on the compressed air pipe assembly with visual activation indicators connected to the air tank outside of the test building. The inspection results reveal that the shutoff valves performed satisfactorily in response to all the earthquake motions. The shutoff valves at level 1 were not triggered during the service level motions. This is due to the fact that the seismic excitations were very low during these low-intensity motions (the peak acceleration < 0.1 g at the first floor).

Table 5.7. Performance of the seismic gas shutoff valves during the pre-fire earthquake tests.

<i>Inspection stage</i>	<i>California Valve (Model 300) Level 1</i>	<i>Little Firefighter (Model AGV-75) Level 1</i>	<i>California Valve (Model 300) Level 6</i>	<i>Little Firefighter (Model AGV-75) Level 6</i>
Post-EQ3	GREEN (active)	GREEN (active)	RED (shut off)	RED (shut off)
Post-EQ5	N/A	N/A	N/A	N/A
Post- EQ6	RED (shut off)	RED (shut off)	RED (shut off)	RED (shut off)
Post- EQ7	RED (shut off)	RED (shut off)	RED (shut off)	RED (shut off)

6 CONCLUSIONS

A substantial growth in the use of cold-formed steel (CFS) framed construction has recently been observed, notably in high seismic regions in the western United States. Structural systems of this kind consist of light-gauge framing members (e.g., studs, tracks, joists) attached with sheathing materials (e.g., wood, sheet steel). CFS-framed structures can offer lower installation and maintenance costs than other structural types, particularly when erected with prefabricated assemblies. They are also durable, formed of an inherently ductile material of consistent behavior, lightweight, and manufactured from recycled materials. Compared to other lightweight framing solutions, CFS is non-combustible, an important basic characteristic to minimize fire spread. While these lightweight systems provide the potential to support the need for resilient and sustainable housing, the state of understanding regarding their structural behavior in response to extreme events, in particular earthquakes and ensuing hazards, remains relatively limited.

To advance knowledge regarding the multi-hazard performance of mid-rise CFS construction, a full-scale six-story cold-formed steel building was constructed and tested on the UCSD Large High Performance Outdoor Shake Table test facility between April and July 2016. The test building was subjected to a suite of seven earthquake motions with progressively increasing motion intensity (from service to MCE level). Following the first seven earthquake tests, live fire tests were conducted on the earthquake-damage building in six strategically selected rooms to evaluate the performance of fire protection systems and the impact of seismic damage of the building and the associated characteristics of the fires that ensued. The test program concluded with two earthquake tests following the fire tests, the final being a high intensity MCE-scaled near-fault motion. Key findings from this test program are summarized as follows:

1. *Pre-fire Earthquake Tests*: The test building suffered minimal damage during the service level earthquake tests and remained largely in the quasi-linear range, with very low drift demands imposed on the specimen (interstory drift $< 0.2\%$). During the design level earthquake test, the corridor shear and gravity walls at level 3 and 4 suffered damage in the form of gypsum panel crushing and fastener withdrawal when the interstory drifts at these two levels reached about 1.0%. This is

corroborated by the fact that the building fundamental period increased by more than 50%. Damage continued to progress as the interstory drift exceeded 1.5% during the maximum considered earthquake (MCE) test, however observed damage to the building remained readily repairable, with the structural shearwalls at the lower floors (those that could be inspected) developing their intended local steel sheathing buckling mechanism near attachment points along framing member perimeters. The building structural components performed satisfactorily throughout the pre-fire earthquake test sequence. The most significant damage to the structural system, as noted, occurred in the form of buckled sheet steel on the corridor shear walls composite panels. The pre-fire earthquake test sequence however do highlight the potential risk of fuel and fire ignition following the earthquakes, as the various appliances placed in the building were prone to large movements, bracing or restraint failure, and tipping in some cases.

2. *Fire Tests:* Post-flashover conditions were achieved in all six compartment fire tests at the given ventilation conditions, with the corresponding maximum compartment temperatures ranging between 800 °C and 1100 °C (four out of six tests exceeding 1000 °C). The elevated temperature caused significant degradation of interior fire rated gypsum wallboards on sheet steel and plain fire rated gypsum wallboards sans sheet steel, leading to loss of structural strength. Loss of rigidity in floor sheathing due to degradation of cement board on top of the sheet steel caused significant floor deflections (about 1.5 cm). Thermal bowing of floor joists was observed after the test suggesting that there was a significant flow of heat from the floor system under consideration. The dehydrated and detached ceiling panel may cause potential overhead hazards in the case of an aftershock event, and the extended flames through the building exterior openings also emphasize that the high likelihood of travelling fire hazards. It is recommended that further investigation be conducted to assess the fire performance of light-gauge buildings with realistic architectural features (glazed windows, exterior and interior wall finishes) and appliances.
3. *Post-fire Earthquake Tests:* The low-amplitude aftershock significantly attenuated seismic demands in the building as a result of the elongated period caused by the

pre-fire earthquake sequence. In contrast, the extreme near-fault earthquake test (EQ9) developed a full soft story mechanism at level 2 and caused severe damage to the buildings structural system (complete loss of structural integrity of corridor and exterior longitudinal shear walls). The test building resisted collapse due to redistribution of loads and framing action of the building rod tie-down system.

REFERENCES

- AISI (American Iron and Steel Institute) (2007). *North American Standard for Cold-formed Steel Farming—Lateral Design*. AISI S213, Washington DC.
- AISI (American Iron and Steel Institute) (2012a). *North American Specification for the Design of Cold-formed Steel Structural Members*. AISI S100, Washington DC.
- ASCE (American Society of Civil Engineers) (2010). *Minimum Design Loads for Buildings and Other Structures*. ASCE 7, Reston, VA
- Bock, Y., Melgar, D., and Crowell, B.W. (2011). “Real-time strong-motion broadband displacements from collocated GPS and accelerometers.” *Bulletin of the Seismological Society of America*, 101(6), 2904-2925.
- Goldberg, D., and Bock, Y. (2016). *Shake Table Experiments GPS Deployments: June-July, 2016*. Scripps Orbit and Permanent Array Center, La Jolla, CA
- Hoehler, M., and Smith, C. (2016). Influence of Fire on the Lateral Load Capacity of Steel-sheathed Cold-Formed Steel Shear Walls – Report of Test. *NISTIR 8160*, National Institute of Standards and Technology, Gaithersburg, MD
- Skolnik, D.A. and Wallace, J.W. (2010). “Critical assessment of interstory drift measurements.” *ASCE Journal of Structural Engineering*, 136(12), 1574–1584.
- van Overschee, P. and De Moor, B. (1996). *Subspace Identification for Linear systems: Theory, Implementation, Applications*. Kluwer academic publishers, Boston, MA.

APPENDIX A – PROJECT PARTICIPANTS

Table A.1. Project academic team

<i>Name</i>	<i>Title</i>	<i>Affiliation</i>
Tara Hutchinson	Professor (PI)	University of California, san Diego
Gilbert Hegemier	Professor (co-PI)	University of California, san Diego
Brian Meacham	Associate Professor	Worcester Polytechnic Institute
Xiang Wang	Postdoctoral Researcher	University of California, san Diego
Praveen Kamath	Postdoctoral Researcher	Worcester Polytechnic Institute
Srikar Gunisetty	Graduate Researcher	University of California, San Diego
Daniel Arthur	Research Assistant	Worcester Polytechnic Institute

Table A.2. Government and institutional sponsors

<i>List of Sponsors</i>
Department of Housing and Urban Development
California Seismic Safety Commission
Jacobs School of Engineering, University of California, San Diego
Department of Fire Protection Engineering, Worcester Polytechnic Institute

Table A.3. Industrial sponsors

<i>Company Name</i>	<i>Primary Contact</i>
Allegion	Tim Weller
CEMCO Steel	Fernando Sesma
DCI Engineers	Harry Jones
DPR Construction	Steve Helland
Insurance Institute for Business & Home Safety	Tim Reinhold
MiTek Structural Connectors	Jesse Karns
Rivante	Douglas Antuma
Society of Fire Protection Engineers (SFPE) Foundation	Maggie McGray
Southwest Carpenters Union	Thomas Rooney
State Farm Insurance	Pat Boyer, Jack Jordan, Larry Stevig
Suffolk Construction	Andrew Carniff
Sure-Board	Kelly Holcomb
SWS Panel	Diego Rivera
USG Building Materials	
United Scaffold, Inc.	Greg Leonard
Walters & Wolf	Rick Calhoun

APPENDIX B – SHAKE TABLE SPECIFICATIONS

The UCSD Large High Performance Outdoor Shake Table (LHPOST) is the largest outdoor shake table in the world and the largest shake table of its kind in the United States (Figure B.1). This experimental facility is currently operated within the Natural Hazards Engineering Research Infrastructure (NHERI) equipment inventory. Uniquely, it enables seismic testing of large scale and/or full-scale structural or geotechnical systems with realistic earthquake loading, extensive instrumentation and data archiving. This testing site is essential for capturing system responses of the full-scale tests that cannot be achieved at smaller scales.



Figure B.1. UCSD Large High Performance Outdoor Shake Table (LHPOST).

As shown in Figure B.2, the LHPOST test facility is composed of several essential components:

- A moving steel platen with it dimension of 7.6m x 12.2m and a weight of ~1700 kN.
- A reinforced concrete reaction mass block
- Two servo-controlled dynamic horizontal actuators equipped with high flow servo-valves to power the shake table
- A platen sliding system consisting of six vertical actuators to react against all vertical forces with very low friction allowing the table to operate at a high stroke and velocity capacity
- Two nitrogen-filled hold down struts to resist overturning moments
- A yaw restraint system consisting of two pairs of slaved hydrostatic pressure-balanced bearings

With the velocity, stroke capabilities, and the frequency bandwidth as summarized in Table B.1, the shake table is capable of accurately reproducing severe near-fault earthquake ground motions even for very large structural systems (nheri.ucsd.edu).

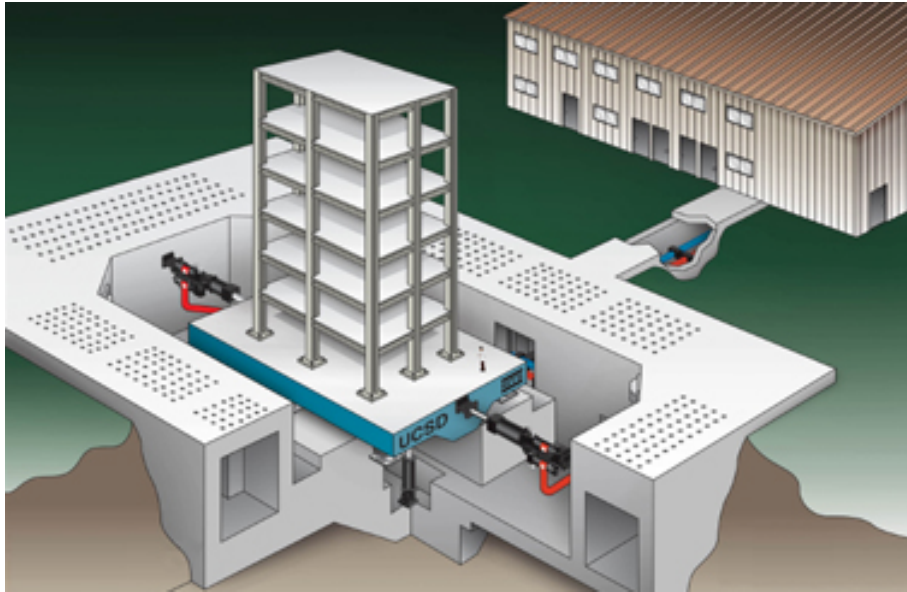


Figure B.2. Schematic view of the LHPOST test facility (nheri.ucsd.edu).

Table B.1. Shake table performance specifications

Dimension	7.6 m x 12.2 m
Peak acceleration: bare table (400 ton payload)	4.2 g (1.2 g)
Peak velocity	1.8 m/s
Displacement stroke	± 0.75 m
Maximum (vertical) payload	20 MN
Force capacity of actuators	6.8 MN
Maximum overturning moment: bare table (400 ton payload)	35 MN-m (50 MN-m)
Frequency bandwidth	0-33 Hz

APPENDIX C – TEST DAY PROTOCOL

TEST DAY 1 (06/13/2016)

No.	Type of test	Sampling rate (Hz)	Starting time (PST) – Duration (sec)
1	1.5% g RMS white noise for building warm up and sensor engagement (1 min)	240	
2	0.08 g pulse	240	
3	1.5% g RMS white noise (3 min)	240	
4	3.0% g RMS white noise (3 min)	240	
5	25% RIO360 – service level (EQ1)	240	11:11:00 – 60
6	1.5% g RMS white noise (3 min)	240	
7	25% CNP196 – service level (EQ2)	240	11:36:54 – 60
8	1.5% g RMS white noise (3 min)	240	
building inspection & quick data check (table down)			
9	1.5% g RMS white noise for building warm up and sensor engagement (1 min)	240	
10	25% CUREW – service level (EQ3)	240	14:19:53 – 200
11	0.08 g pulse	240	
12	1.5% g RMS white noise (3 min)	240	
13	3.0% g RMS white noise (3 min)	240	

TEST DAY 2 (06/15/2016)

No.	Type of test	Sampling rate (Hz)	Starting time (PST) – Duration (sec)
1	1.5% g RMS white noise for building warm up and sensor engagement (1 min)	240	
2	0.08 g pulse	240	
3	1.5% g RMS white noise (3 min)	240	
4	3.0% g RMS white noise (3 min)	240	
5	25% CNP196 – service level (EQ4)	240	10:05:51 – 60
6	0.08 g pulse	240	
7	1.5% g RMS white noise (3 min)	240	
8	3.0% g RMS white noise (3 min)	240	
building inspection & quick data check (table down)			
9	1.5% g RMS white noise for building warm up and sensor engagement (1 min)	240	
10	50% CNP196 – 50% design level (EQ5)	240	12:35:06 – 60
11	1.5% g RMS white noise (3 min)	240	
12	3.0% g RMS white noise (3 min)	240	
13	100% CNP196 – design level (EQ6)	240	13:00:51 – 60
14	0.08 g pulse	240	
15	1.5% g RMS white noise (3 min)	240	
16	3.0% g RMS white noise (3 min)	240	

TEST DAY 3 (06/17/2016)

No.	Type of test	Sampling rate (Hz)	Starting time (PST) – Duration (sec)
1	1.5% g RMS white noise for building warm up and sensor engagement (1 min)	240	
2	0.08 g pulse	240	
3	1.5% g RMS white noise (3 min)	240	
4	3.0% g RMS white noise (3 min)	240	
5	150% CNP196 – MCE level (EQ7)	240	11:35:04 – 60
6	0.08 g pulse	240	
7	1.5% g RMS white noise (3 min)	240	
8	3.0% g RMS white noise (3 min)	240	

TEST DAY 4 (07/01/2016)

No.	Type of test	Sampling rate (Hz)	Starting time (PST) – Duration (sec)
1	1.5% g RMS white noise (3 min)	240	
2	3.0% g RMS white noise (3 min)	240	
3	25% RIO360 – service level “aftershock” (EQ8)	240	09:41:52 – 60
4	1.5% g RMS white noise (3 min)	240	
5	3.0% g RMS white noise (3 min)	240	
building inspection & quick data check (table down)			
6	1.5% g RMS white noise for building warm up and sensor engagement (1 min)	240	
7	150% RRS228 – near-fault MCE level (EQ9)	240	11:25:13 – 60